A NUMERICAL STUDY IN THE DEVELOPING REGION OF COAXIAL AXISYMMETRIC CONFINED JET

by

RABINDRA NATH PAUL
B. Sc. Engineering (Mechanical)

Thesis Submitted to the
Department of Mechanical Engineering in Partial Fuifilment
of the Requirements for the Degree of
Master of Science
in
Mechanical Engineering

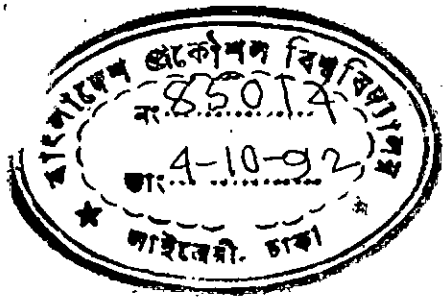

Bangladesh University of Engineering and Technology
Dhaka, Bangladesh
July, 1992

A NUMERICAL STUDY IN THE DEVELOPING REGION OF COAXIAL AXISYMMETRIC CONFINED JET

A Thesis
by
Rabindra Nath Paul

Approved as to Style and Content:

R. G. M. Hasan

(Dr. R. G. M. Hasan) — Chairman
Assistant Professor
Dept. of Mechanical Engineering
BUET, Dhaka-1000.

(Dr. Md. Wahhaj Uddin) — Member(Ex-Officio)
Professor & Head
Dept. of Mechanical Engineering
BUET, Dhaka-1000.

(Dr. A.K.M. Sadrul Islam) — Member
Associate Professor
Dept. of Mechanical Engineering
BUET, Dhaka-1000.

(Dr. Md. Abdul Matin) — Member(External)
Assistant Professor
Dept. of Water Resources Engineering
BUET, Dhaka-1000.

ABSTRACT

The flow characteristics in the developing region of coaxial axisymmetric confined jets were studied numerically. The computer programme used for this purpose employed finite volume discretisation of Navier-Stokes equations and a two-equation (k-ε) turbulence model. After sufficient testing against bench-mark experimental and analytical data, the computer programme was used for the prediction of coaxial jet.

The present study is confined to jets of a fixed diameter ratio of 2.48. To study the effect of boundary layer at primary jet exit, four different velocity profiles were considered. The Reynolds number and the velocity ratio were kept unchanged for these four cases and were taken to be 3.28×10^4 and 0.023, respectively. Then, for the same Reynolds number, the flow development was studied for four different velocity ratios viz., 0.05, 0.1, 0.2 and 0.5. Finally, the Reynolds number was increased to 3.28×10^5 and for a velocity ratio of 0.5 computations were made for two inlet profiles.

It is found that recirculation phenomena, growth rate of jet and turbulence intensity distinctly depend on the shear layer of velocity profile at primary nozzle exit. However, pressure is rather insensitive to inlet profile variation. For higher velocity ratios (>0.023) recirculation does not occur and the turbulence intensity is found to be suppressed. It is further seen that the flow assumes a self preserving profile in the later part of the developing region.

ACKNOWLEDGEMENTS

The author would like to express his sincerest gratitude and indebtedness to his Supervisor, Dr. R. G. M. Hasan, Assistant Professor, Department of Mechanical Engineering, BUET, Dhaka for his guidance, constant encouragement and invaluable suggestions all through the working period on this project and also for his ever friendly and patient attitude in achieving every minute detail of this thesis.

The author is also very grateful to Dr. Md. Wahhaj Uddin, Professor and Head, Department of Mechanical Engineering, BUET who provided all necessary assistance in various ways at different stages of the work.

The author is highly grateful to Dr. A. C. Mandal and Dr. A. K. M. Sadrul Islam for their constructive suggestions and continuous encouragement during this investigation.

Sincere thanks are offered to Dr. S. R. Husain and Md. Maniruzzaman for their constant assistance and suggestions in running the computer programme.

Finally, the author would like to thank his wife who persistently kept him at his work and relieved him from most of the family duties while this work was continuing.

TABLE OF CONTENTS

LIST OF FIGURES

LIST OF TABLES

NOMENCLATURE

SYMBOL MEANING

Latin Letters

A	Cross-sectional area
C_t	Craya-curtet number
D	Diameter
g	Acceleration due to gravity
H^1	Dimensionless characteristic parameter = $Q/\sqrt{W/\rho r_t}$
H	Shape factor, Characteristic jet parameter
k	Local kinetic energy
l	Characteristic length
m	Similitude parameter
P	Static pressure
P^*	Non-dimensional pressure rise = $\frac{P-P_o}{.5\rho U_o^2}$
Q	Flow rate
R	Non-dimensional radial distance = r/r_t
r	Radius, radial direction
$R_{1/2}$	Radius at which velocity is half of the center-line velocity $(u - u_s) = 0.5\ (u_c - u_s)$
$r_{1/2}$	Half radius.

SYMBOL	MEANING
S	Secondary stream
u	Local axial mean velocity
U	Free stream velocity
$\overline{U}$	Area mean velocity
U'	Local turbulence intensity = $\sqrt{\frac{2k}{3}}$
v	Radial velocity
w	Pressure plus momentum integral at any section.
t	Of mixing pipe
w	At wall
x	Axial direction
X	Non-dimensional axial location = x/r_t

GREEK SYMBOLS

δ^*	Displacement thickness normalised by r_n
θ	Momentum thickness normalised by r_n
ρ	Density
Γ	Diffusion coefficient
Ψ	Stream function
μ	Absolute viscosity
ε	Dissipation quantity

SYMBOL MEANING

SUBSCRIPTS

n	Jet Nozzle
o	Jet Exit
p	Primary stream
s	Secondary stream
t	Mixing tube, turbulent quantity

CHAPTER I

INTRODUCTION

1.1 Background

A jet is formed when a fluid is discharged through a nozzle or an orifice from a region of higher pressure to a region of lower pressure. Jets are broadly classified into three categories: (a) Free Jet, if it expands freely in an infinite fluid; (b) Wall Jet, if the jet impinges on a rigid wall, and (c) Confined Jet, if it expands in a confined space such as a conduit. These three jets are shown schematically in Fig.1.1.

All the above three categories of jets are commonly encountered in many practical engineering applications. For example, the exhaust from an engine is expelled into the atmosphere in the form of a free jet and the fluid flow in the Pelton wheel is a classic example of a wall jet. Confined jets are encountered in the design of water jet pumps, furnaces, steam-jet ejector of air-conditioning plants, etc.

Like the other two types of jets, confined jet has been the prime attention as a subject of research for a long time. Specially, during the last two or three decades, the environmentalists' pressure has forced different industrialised nations to cut down the level of NOX (NO, NO_2 etc.) and unburned fuel emissions from furnaces. Since these harmful substances are the direct result of combustion, the research

work on confined jets has also increased during the last two decades. In this thesis, some aspects of confined jet have been studied and presented.

1.2 The Coaxial Confined Jet

The most common confined jet is a circular jet such as the one shown in Fig. 1.1c. If this jet is surrounded by another concentric jet, it is termed as coaxial confined jet. Like other practical fluid flows, confined jets are also mostly turbulent in nature. This type of jet is the subject of study of the present thesis. Its schematic diagram is shown in Fig.1.2.

The diagram shows a circular jet of diameter $D_n = 2r_n$, issuing axially into a duct of diameter $D_t = 2r_t$, with a uniform velocity of U_p. This jet is generally known as the primary stream, and hence U_p is called the primary stream velocity. The surrounding fluid is also in motion in the direction of primary jet at the exit plane of the nozzle edge, and is known as the secondary stream. Here U_s represents the secondary stream velocity.

It can be clearly seen that the primary stream and the secondary stream form a coaxial axisymmetric confined jet.

Generally, the flow field of coaxial axisymmetric confined jet may be divided into three different regions[26],* each having different flow characteristics. The initial region, region 1, consists of two different potential flow regions and two different

* All superscript numbers are reference number.

shear flow regions. One shear flow region exists between the jet and the secondary flow and another near the wall. The shear zone near the jet spreads both inward and outward decreasing the jet potential flow zone and secondary potential flow zone.

In region 2, the central potential flow region no longer exists. The outer potential flow region does exist but continues to decrease in size. The velocity profiles in this region may tend to maintain similar shape.

In region 3, the boundary layer has merged with the jet. Thus no portion of the velocity profile is uniform in this region. The velocity profile continues to change until the flow becomes fully developed. This region is generally much longer than either of the two other regions.

Basically, the confined jet has some of the features of a free jet and some of the features of duct flows. One of the fundamental differences between the free and the confined jet, however, is that the existence of the confining walls in confined jet causes an axial pressure gradient. The effect of the pressure gradient is to modify the rate of spread of the jet, rate of growth of the boundary layer and hence the shape of the velocity profile. Such features along with other critical flow parameters will be discussed later in this thesis.

1.3 Critical Parameters of the Confined Jet

The works reported in this thesis is based on the numerical solution of Navier-Stokes equations* subject to appropriate boundary conditions of coaxial axisymmetric confined jet. For the analysis of the problem, several parameters were defined which are now described below.

Diameter or Radius Ratio: It is the ratio of the diameter of the pipe (mixing tube) to that of the nozzle, D_t/D_n.

Velocity Ratio: It is the ratio of secondary stream velocity to the primary stream velocity, U_s/U_p.

Nozzle Reynolds Number: The Reynolds number at nozzle exit is based on the area-mean velocity of primary jet and the diameter of the nozzle. It is defined as,

$$Re_n = \frac{\rho \bar{U}_p D_n}{\mu} \qquad [1.1]$$

Where ρ is the density and μ the absolute viscosity of the fluid.

---

* The detailed methodology is described in Ch. 3,

In this thesis the velocity profile of the primary stream at the entry to the duct considered to be is an important parameter. A convenient way to quantify such boundary layer is the inlet shape factor. This is defined as the ratio of displacement thickness to the momentum thickness of the boundary layer. Symbolically,

$$\text{Shape factor, } H = \frac{\delta^*}{\theta} \qquad [1.2]$$

The displacement thickness δ^* of the boundary layer is the distance through which the actual boundary would have to be displaced in order that the actual flow rate is the same as that of an ideal fluid flowing over the displaced boundary.

The momentum thickness θ of the boundary layer is the distance from the actual boundary such that the momentum flux through the distance θ is the same as the deficit of the momentum flux through the actual boundary layer.

The shape factor of a boundary layer is an indication of whether a boundary layer is laminar or turbulent. For fully turbulent flow, the shape factor is usually found to be between 1.3 - 2.2.

1.4 Outline of the Thesis

The remaining part of the thesis is divided into four Chapters. First, in Chapter 2, relevant literature is briefly reviewed in order to highlight the trend of research in this field. The objectives of the present work are also given at the end of the next chapter.

It is mentioned earlier that the present work is a numerical study. The basic governing equations and the method of solution of this study are outlined in Chapter 3.

The results and discussions are presented in Chapter 4 and finally in Chapter 5 the findings of the thesis are summarized. Some suggestions for future work are also mentioned in this chapter.

References and figures are presented at the end of the thesis.

CHAPTER II

LITERATURE SURVEY

2.1. Introduction

The study of confined jet is an important area of research for the last few decades. Several authors have studied the flow characteristics with different fluids and different geometrical configurations. The common fluids are air and water, but the works employing air far outnumber the works with any other fluid. The possible reasons may be that (a) the air jets are more commonly encountered in practical engineering applications and that (b) it is easier to handle an experiment with air in an ordinary research laboratory.

The most common geometry is the concentric annular jet as shown in Fig. 1.2 (which is also the geometry of the present investigation). Apart from this, various other geometrical shapes such as inclined primary jet, converging and diverging mixing tube, double concentric jet, etc., are also found in the literature. Some of these less common geometries were studied by Mahmud[21], Agrawal et al[1] and others.

2.2 Previous Works

Razinsky and Brighton[27] studied experimentally the confined jet in ducts of diameter ratio $D_t/D_n = 3$ and 6. They measured (i) Wall static pressure, (ii) Mean velocity, (iii) Turbulence intensity and Reynolds stress throughout the flow field. Experiments were done for velocity ratios of 0.1, 0.167, .335, 0.5 and 0.67. Razinsky pointed out that the pressure gradients for velocity ratios of 0.5 and 0.67 are favourable whereas for low velocity ratios the axial pressure distribution increased in the early mixing region, reaching a maximum at about 13 radii from nozzle exit, then decreased over the remaining portion of the mixing tube. The fully developed pressure gradient was reached at about 20 radii, long before the fully developed mean velocity profiles. For high velocity ratios, the pressure decreased right from the inlet.

Of the five velocity ratios the authors found that separation occured only for the lowest velocity ratio i.e., $U_s/U_p = 0.1$. They observed flow separation between axial distances of 3.5 and 5.5 radii. In a later experimental study by Hasan[11], this type of recirculation has also been mentioned.

It has been found that the potential core was quickly consumed by the jet shear layer i.e., within 1 to 3 radii from inlet. This length of the jet core has been observed to depend on velocity ratio for a given radius ratio. It was found that the lower the velocity ratio, the shorter the length of the jet core. On the other hand, the uniform secondary velocity i.e., secondary potential core existed for a

longer length than the primary, but it too was found to be shorter for lower velocity ratio.

The work of Razinsky and Brighton[27] is very detailed especially for turbulence quantities. The authors found that the entrance turbulence intensity profiles were composed of a uniform low intensity primary jet (about 1 percent) and a low intensity secondary jet (about 3 percent).

In region 1 (see Fig. 1.2) turbulence intensities are low near the centre line. Low intensity near the wall existed upto 2/3 pipe radius from the entrance, indicating nonturbulent boundary layer. After 2/3 radius from the entrance, the intensity was found to be high which is an indication of fully turbulent boundary layer. In region 2 a sharp rise in the centre line turbulence was observed. At 14 radii the intensity zone of the jet disappeared and the profile became similar to the fully developed pipe flow (increasing from center line to the wall). Upto about 65 radii the centre line intensity was found to decrease and then the high intensity zone due to the wall boundary layer become the dominant factor in determining the intensity profile.

They further observed that for low velocity ratio i.e., $U_s/U_p = 0.1$, the turbulence intensity profiles are somewhat different. In this case, zone of high intensity occurs in a short region of recirculation. Further downstream of the separation, the intensity profiles are similar to those of the nonseparated cases.

In a contemporary study by Durao and Whitelaw[8], turbulent mixing in the developing region of co-axial jets are presented. The measurements were obtained with three velocity ratios U_s/U_p = 1.61, 4.34 and ∞ and at a downstream distance of upto 34 radii. In this study the authors took the initial conditions of the primary stream corresponding to the fully developed pipe flow and annulus flows with significant separation between the two streams. This initial condition is different from that of Razinsky and Brighton[27] in which they used continuous coaxial stream, not annular. The velocity ratio $U_s/U_p > 1$ was used by the authors which is also different from Razinsky's. The velocity ratio $U_s/U_p > 1$ was chosen because of the reason that these velocity ratios ensure rapid mixing. The study indicates that velocity ratio of infinity (∞) leads to the most rapid mixing, because low initial value of U_p causes a significant fall in the magnitude of U_p near the entrance which results in quick entrainment of secondary stream into the primary stream.

The results also demonstrate that coaxial jets reach a self preserving condition similar to that of an axisymmetric jet (Hinze[15]) but attain this state more rapidly. The mean velocity, normal and shear stresseš will become asymptotic to this self preserving state at the same down-stream location. For the particular geometry investigated, a velocity ratio of 6.67 corresponds to the slowest rate of development.

They also indicate that the relative magnitude of three normal stress (in three directions) varies significantly in the developing region which indicates the

unsatisfactory nature of kinetic energy. Detailed turbulence data are not reported in this work.

Champagne and Wygnanski[5] performed an experimental investigation of coaxial turbulent jets. Measurements were taken by hot wire anemomenters for two diameters ratios (D_t/D_n = 1.13 and 1.714) and for three velocity ratios (U_s/U_p = 0.5, 1.5 and 10). The distribution of the mean velocities, turbulence intensities, and shear stresses were determined for the various cases. The Reynolds numbers based on the nozzle diameter varied in the range of 10^5. Effect of variation of inlet velocity profile are not reported in this work.

Champagne et al pointed out that close to the nozzle exit, the flow consist of two potential cores and two mixing regions. The width of the each core decreases with downstream distance. This idea was also reported by Razinsky and Brighton[27]. The length of the external core appears to be independent of the velocity ratio U_s/U_p. On the other hand, the length of the inner core, strongly depends on U_s/U_p and D_t/D_n. The effect is particularly significant for $U_s/U_p > 1$, because in this case low pressure created in inner core bends the outer jet inwards. So for $U_s/U_p > 1$, the length of the inner core reduced rapidly.

For $U_s/U_p < 1$, no such effect was observed and the termination of the interior core results in a continuous reduction of maximum axial mean velocity.

Champagne and Wygnanski[5] also examined the distribution of axial and radial turbulence intensities for different velocity and diameter ratio. They have observed that the distribution of the turbulence intensities are closely related to the shape of the mean velocity profile. Turbulence intensities in the initial region were found smaller for $U_s/U_p = 0.5$, than for $U_s/U_p = 5$ whereas inner potential core was smaller for $U_s/U_p = 5$ than for $U_s/U_p = 0.5$. They finally conclude that for a fixed diameter ratio, velocity ratio U_s/U_p should be greater than one to enhance rapid mixing between the two streams.

Kwan and Ko[18] investigated experimentally the initial region of subsonic coaxial jets. In part 1 of their investigation they suggested that coherent structures in the form of two different arrays of vortices, exist in the initial region of coaxial jets. In part 2 of their study, in order to obtain further information on the characteristics of the vortices in coaxial jets, single and two point correlation covariance measurements of the fluctuating pressure and velocity were made in the initial region of coaxial jets. From the correlation results, the phase properties obtained within the whole initial region of coaxial jets were found to agree with the results for single jets.

A theoretical investigation has been carried out by Azim[2] for flows in the developing region of coflowing axisymmetric turbulent jets. The calculations were performed for velocity ratio $U_s/U_p = 0.0$, 0.1 and 0.25 with a constant temperature ratio (defined as the ratio of temperature at the outer edge of jet to that of exit) 0.3 for each case. Mean velocity and mean temperature in the initial and

transition region were calculated. He also studied the suitability of length scale for the description and analysis of the flow.

His finding reveals that growth of half-radii $R_{1/2}$ for lower velocity ratio is higher than that for high velocity ratio. Length of the potential core was found to increase with increase of velocity ratio. According to him, a self-preserving model with shear layer thickness as a length scale is not suitable because the highest experimental uncertainity occurs near the outer boundary where the mean velocity is low. In developing a self-preserving model it was found that half radius can be considered to be a suitable length scale.

Hasan[11] studied experimentally the flow characteristics along the downstream of an axisymmetric jet issuing axially into a smooth pipe. This study is different from the works of Razinsky and Brighton[27] and Durao and Whitelaw[8] etc., that various types of inlet profiles were used to see the effects of inlet profile on flow development. Profiles 2, 3 and 4 as shown in Fig. 4.3b-d were used to study the effect of variation of boundary layer thickness. Reynolds number was defined on the basis of diameter of the nozzle and the area mean velocity at nozzle exit. Different Reynolds numbers considered by him were 2.39×10^4, 3.28×10^4, 4.24×10^4 and 5.51×10^4.

The variation of static pressure along the mixing pipe was studied and maximum pressure was observed near the section where the jet attached to the wall. The rate of induced flow was determined for different Reynolds number and boundary

layer thickness at nozzle exit. The maximum induced flow was found to be 21.95% and it occured at Re_n = 3.28 X 10^4 and for inlet profile 4. The zone of attachment of the jet with pipe was found to be between x/r_t = 5.5 to 7.5. It was found from his experiment that after the jet attached to the wall, the flow pattern along the downstream was a developing turbulent pipe flow.

This study did not report any turbulence data because of the limitation of experimental facility. Never-the-less the main motivation for the present study is obtained from the experimental study by Hasan[11]. As he considers the different inlet velocity profiles to study the effects on flow development, the present prediction will be compared with those of Hasan[11] by using the same inlet velocity profiles.

The essential feature of the coaxial axisymmetric confined jet have also been studied by many other investigators and these features are summarized by Rajaratnam[26]. To describe the characteristic feature the author used some confined jet parameters such as H^1, C_t and m. Here H^1 is a dimensionless characteristic parameter combining W, Q and other relevant variables describing this phenomenon. H^1 is defined as

$$H^1 = \frac{1}{\sqrt{2\pi}} \quad \frac{Q}{\sqrt{W/\rho R_t}} \qquad [2.1]$$

Here W denotes the pressure plus momentum integral at any section.

Q denotes flow rate

ρ = density and R_t = radius of the pipe.

This form of H^1 was suggested by Hill[14]. The relation between H^1 and other two parameters m and C_t, suggested respectively by Curtet and Ricou[6] and Becker et al.[4] could be reduced to the form given below

$$H^1 = 1/\sqrt{1 + 2/C_t^2} = 1/\sqrt{2\left(m + \frac{1}{2}\right)} \qquad [2.2]$$

The similitude parameter $m = \frac{1}{C_t^2}$ is a nondimensional measure of the weighted momentums of the primary and secondary stream. The Craya-Curtet number C_t is also a nondimensional measure of the relative weightage of the two streams. These parameters H^1, m and C_t have been found to be very useful in describing and predicting the behaviour of confined jet. C_t is also useful for similarity analysis i.e., self preservation.

Apart from the works mentioned earlier, there has been quite a few more works such as Hill[14], Hembold et al.[12], Mikhail[22], Becker et al.[4], Dealy[7], Curtet and Ricou[6], Barchilon and Curtet[3], and others. The significant findings of these works along with others are given in Table 1.1.

TABLE 1.1: Significant Details of the Experiments on Circular Confined Jets.

	Investigators	Significant Details of the Experiments
a	**Ko and Lam[17]**	**D_t/D_n = 2 U_s/U_p = 0.5**
b	Hasan[11]	D_t/D_n = 2.5 U_s/U_p = 0.023
c	Exely and Brighton[9]	D_t = 6 in., D_t/D_n = 6.3 and 2.0, U_s/U_p from 0.03 to 0.211
d	Durao and Whitelaw[8]	D_t/D_n = 2.4, U_s/U_p = 1.61, 4.34, ∞
e	Champagne and Wygnanski[5]	D_t/D_n = 1.13, 1.714 U_s/U_p = 1, 5, 10.
f	Razinsky and Brighton[27]	D_t = 6 in., D_t/D_n = 3 and 6, U_s/U_p = 0.1, 0.167, 0.333, 0.5 and .067 includes turbulence measurements.
g	Hill[14]	D_t = 2.0 in., D_t/D_n = 8.0, H^1 = 0
h	Barchilon and Curtet[3]	D_t/D_n = 13.4, m from 1.05 to 176.6 and C_t from 0.075 to 0.976.
i	Curtet and Ricou[6]	D_t/D_n = 13.5, m from 0.0083 to 0.57 and C_t from 1.325 to 11.
j	Dealy[7]	D_t = 2.0 in D_t/D_n = 4.0 C_t from 0.251 to 1.54 D_t/D_n = 2.0, C_t from 0.5 to 1.21.
k	Becker et al.[4]	D_t = 19.7cm, D_n = 0.635cm, C_t from 0.033 to 1.22 D_t/D_n = 31.
l	Mikhail[22]	D_t = 4.0 in. U_p = 73 m/s, U_s/U_p 0.125 to 0.222, no recirculation observed.
m	Hembold et al.[12]	D_t = 6.0 in., D_t/D_n = 10, H^1 from 0.209 to 0.734.

It has been found from the available experimental observations that for H^1 less than a critical value of say H_c (or C_t less than a critical value of C_{tc} or m greater than a critical value of m_c), a zone of recirculation or eddy appears in the duct. Barchilon and Curtet[3] suggested that $C_{tc} \approx 0.976$ and Becker et al.[4] found that $C_{tc} \approx 0.75$. The available measurements on the critical values show that C_{tc} is about 1.06 for low values of diameter ratio D_t/D_n and for larger diameter ratio decreases to about 0.732.

Mahmud Truelove and Wall[21] studied the flow characteristics of swirling coaxial jets from divergent nozzles. They studied the aerodynamic characteristics of free, swirling, coaxial jets issuing from an air model of typical burner. Mean velocity and static pressure near the nozzle exit were measured. In order to quantify the effects of velocity ratio and swirl in the primary and secondary jets they identify the boundary of the reverse-flow zone and measured the recirculated mass flow rate. They reported that the type of flow pattern depends upon the level of swirl in primary and secondary jets and the recirculated mass flow rate is predominantly influenced by secondary swirl. The measurements obtained from experiment is compared with the prediction obtained by numerical solution. The computations were done by solving Navier-Stokes equations in two dimensions. Their methodology is similar to the one employed in this thesis.

It has been observed from the comparison with experimental data that the numerical results differ significantly in the regions of high velocity gradient and within the reverse-flow zone. Specially in the reverse-flow zone the mean velocity

was consistantly underpredicted and recirculated mass flow rate obtained from prediction was only one half of those measured.

They concluded that the discrepancies between predictions and measurements were due to measurement error and deficiencies in the turbulence model. They also reported that entrainment and recirculation can not be correctly predicted by the k-ε turbulence model.

In a recent study by Agrawal, Singh and Malhotra[1], the effect of geometrical parameters on the mixing characteristics of coaxial swirling jets are presented. The effect of three expansion shapes, namely sudden expansion, constant angle diffuser and variable angle diffuser expansion, were investigated. Expansion ratio (ratio of exit area to inlet area of the diffuser) for two diffusers was 2 and that for sudden expansion were 1.5, 2 and 3. It was observed that a central recirculation zone forms for all shapes except the sudden expansion with expansion ratio of 2 and 3, for which jet mixing is similar to unconfined flows.

They found the zone of attachment for sudden expansion ratio of 2 and 3 were $2.5r_o$ and $4.5r_o$ and the flow became nearly uniform in those two cases at a distance of $4.5r_o$ and $6.5r_o$ respectively (Here r_o is the radius at the exit of the diffuser). No central recirculation core was observed for the above two expansion ratios. For sudden expansion ratio of 1.5 at $x = .5r_o$, a recirculation was observed. As the fluid flows downstream, central recirculation core (CRC) increases in size.

After attachment of the flow at $x = 2.5r_o$, the flow distributes itself to attain uniformity, limiting the growth of CRC which disappears at around $x = 3.5r_o$.

For the straight diffuser with expansion ratio 2 and shaped diffuser with expansion ratio 2, a CRC appears at near the inlet and disappeared at $x = 9.5r_o$ for both the cases.

The inlet velocity profiles were kept unaltered due to change of shape of the diffuser. Observation of mean velocity profile, turbulence intensity and pressure coefficient P^* at different axial location are also reported. It should be mentioned here that the type of inlet geometry considered in this study is very common in combustors.

Considering the geometrical configuration, the works of Mahmud et al[21] and Agrawal et al[1], are different from all other works mentioned in this chapter. But these are very practical because they simulate the combustors and furnaces. However there are basic similarities with the flows discussed earlier in the section.

2.3. Conclusions Drawn from the Survey:

From the literature survey, it can be observed that although substantial works have been done on confined coaxial jet, the effect of inlet boundary layer on the flow development has not been studied except by one or two authors. Also the

turbulence quantity measurements are reported by only a few authors probably because of limitation of experimental facilities (Durao and Whitelaw[8]).

It may be noted here that a numerical solution is much easier, once the computer programme is sufficiently tested against benchmark experimental data. The advantage is that a large number of parametric studies can be conducted by numerical techniques in a short period of time. This is why the current topic of the thesis has been chosen.

It is therefore obvious that more computational work is necessary in this field. The objectives of the current study are hence presented in the next section.

2.4 Objectives of the Study

Considering the importance of the coflowing confined jets in the field of engineering practice, a research scheme has been undertaken. A fast and reliable computer programme was available to solve the finite-difference equations for given boundary conditions. The flow variables such as velocity component, static pressure, kinetic energy, etc., at different sections of the mixing pipe could be calculated for different input parameters. These parameters are the Reynolds number, velocity ratio of jets, and boundary layer of the velocity profile at the exit of the nozzle. The specific objectives of the present work are-

1. To study the effect of inlet velocity profile at primary nozzle exit on the flow development.

2. To study the effect of Reynolds number and velocity ratio on the flow pattern.

3. To study the static pressure distributions along the downstream of the pipe.

4. To compare the predicted results with available experimental data for establising the reliability of the prediction capacity of algorithm used in this analysis.

CHAPTER III

METHODOLOGY OF NUMERICAL SOLUTION

3.1 Introduction

In this chapter, the methodology of the numerical study is briefly outlined. It is mentioned in the earlier chapters that the flow geometry can be conveniently handled in cylindrical coordinate. Hence the governing differential equations are expressed in cylindrical coordinate and presented in § 3.2. The turbulence model used in this study is a two-equation, k-ε model. The summary of how this model is incorporated in the computer code is also outlined in § 3.2. For the purpose of numerical solution, these equations are to be discretised to equivalent algebraic equations which are then solved by means of some numerical technique of solving algebraic equations. The method of solving algebraic equations are used and hence only a very brief outline is given in § 3.3 along with sufficient references for more information. The boundary conditions are unique for each and every problem and hence they are discussed in § 3.4. Closing remarks are given in § 3.5.

3.2 Governing Equations

The flow geometry considered in this study is axisymmetric and hence a cylindrical mesh is used to cover the flow domain. The governing equations (Navier-Stokes equation) are thus written in cylindrical coordinate with r as the

radial distance and x as the axial distance. There is no angular variation in the present study since the flow is axisymmetric.

The equations governing the particular flow considered in this study are the continuity and momentum equations. All such equations may be represented by one single equation as follows:

$$\frac{1}{r}\frac{\partial}{\partial r}(\rho r v \psi) + \frac{\partial}{\partial x}(\rho u \psi) = \frac{1}{r}\frac{\partial}{\partial r}\{\Gamma r \frac{\partial \psi}{\partial r}\} + \frac{\partial}{\partial x}\{\Gamma \frac{\partial \psi}{\partial x}\} + S_{\psi} \qquad [3.1]$$

In equation (3.1), Ψ may take values 1, u, v and they represent three different equations. The variables v and u are the velocity components in the radial and axial directions respectively (see Fig. 3.1), ρ the density, Γ the diffusion coefficient, equal to the molecular viscosity μ for laminar* flows, and S the source term which is different for different equations as shown in Table 3.1.

The governing equations are described in Appendix - A.

---

* For turbulent flows Γ has a different meaning, described later in the section.

Table 3.1: Source Terms for Different Equations.

Name of Equation	Value of Ψ	source Term, $S\Psi$
Continuity	1	0
u-momentum	u	$-\frac{\partial p}{\partial x} + \frac{1}{r}\frac{\partial}{\partial r}\{\Gamma r \frac{\partial v}{\partial x}\} + \frac{\partial}{\partial x}\{\Gamma \frac{\partial u}{\partial x}\}$
v-momentum	v	$-\frac{\partial p}{\partial r} + \frac{1}{r}\frac{\partial}{\partial r}\{\Gamma r \frac{\partial v}{\partial r}\} + \frac{\partial}{\partial x}\{\Gamma \frac{\partial u}{\partial r}\} - 2\frac{\mu v}{r^2}$

The three equations represented by equation 3.1, form the governing equations for any two-dimensional fluid flow problem if it is not time dependent and the total enthalpy is constant. Hence these equations, when solved with appropriate boundary and initial conditions (to be discussed in §3.4), would in principle provide a complete description of any flow.

Unfortunately, although the above statement is true for laminar flows it is not so for turbulent flows. Because, for turbulent flows, fluctuations of flow variables are always present. Further, with different Reynolds number, there are various ranges

of eddy-size and frequencies present in the flow (Tennekes & Lumley[31]). Therefore, unless special steps are taken, the full three-dimensional time-dependent form of equations are to be solved by employing a very fine mesh with grid-spacing smaller than the characteristic length of the smallest turbulent eddies and time-step small enough to resolve the fastest frequency. This is not at present a practical approach because of the enormous computer time required for such a solution for the high Reynolds number of practical interest.

In order to make the turbulent flow problem amiable to solution, the conventional approach is to obtain equations for `time average' values of random variation. The time-averaging process consists of expressing each variable through its mean value $\overline{\psi}$ and fluctuating component ψ', as

$$\psi = \overline{\psi} + \psi' \qquad [3.2]$$

Now, if Ψ of Eq. (3.1) is decomposed into mean and fluctuating components as in using equation (3.2), then unknown correlations between fluctuating components appear for momentum and scalar quantities which are termed as Reynolds stresses. Although additional equations may be derived for these Reynolds stresses but further unknown are then introduced . This is traditionally known as "closure problem". To overcome this problem of closure of the system of equations, some sort of modelling is necessary. A wide range of turbulence models have been proposed in the literature (Gibson et al[10], Lander and Spalding[19] etc). These vary both in complexity and in the physical realism which they embody. For this study

the most widely used k-ε model of turbulence of Jones and Launder[16] has been used.

Without going into details the model uses a gradient diffusion approximation for the Reynolds stresses i.e., involves a linear stress vs. strain rate relationship analysis to that of Newtonian fluid, with the molecular viscosity replaced by a turbulent or eddy viscosity. The eddy viscosity is calculated by solving two more conservation equations; one for the kinetic energy of turbulence, k and the other for its dissipation rate, ε.

The differential equations for k and ε are exactly of the same form as Eq. (3.1) with the following source terms as given in Table 3.2. The diffusion coefficient Γ is now different which is given by

$$\Gamma = \mu + \mu_t \qquad [3.3]$$

and $$\mu_t = C_\mu \rho k^2/\varepsilon \qquad [3.4]$$

Table 3.2: Source Terms for k and ε Equations.

Name of Equation	Value of Ψ	Source term, S_Ψ
k-equation	k	$G - \rho\varepsilon$
ε-equation	ε	$C_1 \frac{\epsilon}{k} G - C_2 \rho \frac{\epsilon^2}{k}$

In Eq. (3.4) and Table 3.2 Cμ, C_1, C_2 are empirical constants and, according to Launder and Spalding[19], $C_\mu = 0.09$, $C_1 = 1.44$ and $C_2 = 1.92$. G represents the rate of production of turbulent kinetic energy, given by,

$$G = \Gamma[2\{(\frac{\partial v}{\partial r})^2 + (\frac{\partial u}{\partial x})^2 + (\frac{v}{r})^2\} + \{\frac{\partial u}{\partial r} + \frac{\partial v}{\partial x}\}^2] \qquad [3.5]$$

Hence for the solution of turbulent flows, a total of five coupled equations are to be solved viz., continuity, u and v-momentum, k and ε. For all these equations Γ is calculated using Eq. (3.3), whereas for laminar flows only the first three equations were considered with Γ equal to molecular viscosity.

3.3 Solution Technique

The differential equations presented in the previous section are in their exact form. In order that a numerical integration can be carried out, the differential equations are to be transformed first into approximate algebraic equations. To do

this, the flow domain is divided into small control volumes (see Fig. 3.2) where the velocity components are stored on the face of the control volumes. All scalar quantities such as pressure, turbulence intensity and dissipation rate are stored on the grid points. This type of arrangement is called the `staggered' grid arrangement.

The differential equations are then discretised over the cell volume. During the process of discritisation, several assumptions, approximations and convection schemes of Patankar[24] are considered. Since these matters are fairly established and well practised over the last one-and-a-half decade and since all such details are described in Patankar[24], Roache[28] etc., it is felt that these topics may be omitted in this thesis.

The algebraic equations resulting from the differential equations are solved by an iterative technique called Tri Diagonal Matrix Algorithm, (Roache[28]). Typically, the calculations start with an initial guess of the velocity components and turbulence quantities. Pressure is calculated indirectly through a modified form of the continuity equation called the pressure-correction equation* . After one iteration,

---

* It is noteworthy that although there are equations for every velocity component and turbulence quantity, there is no obvious equation for pressure which is also a dependent variable. This can be clearly seen from the pressure gradient term in momentum equations (source terms of Table 3.1). The methodology is to extract the pressure field through pressure correction. In fact this is the main theme of the SIMPLE (Semi-Implicit Pressure Linked Equations) algorithm adopted in the computer code. Some detail of the derivation of pressure correction equation is given in Appendix-B.

the `old' field values of dependent variables such as u, v,p etc., are replaced by the `new' ones and the procedure continues until the convergence is reached.

Convergence was checked by monitoring the total summation of the mass source errors of the control volumes and when the total mass source error reached below 0.1% of the inlet flow the solution was declared converged. In addition to this, the field values of the variables at certain location were monitored and the computer programme was allowed to run until no appreciable change in value was observed. Detailed about computer programme is presented in Appendix - B.

3.4 Boundary Conditions

The flow configuration considered in this thesis is shown in Fig. 3.1 (also in Fig. 1.2). Since the flow is considered to be axisymmetric two-dimensional, the flow field has four boundaries viz., Inflow, Outflow, Solid wall and Symmetry axis. The boundary conditions of these four boundaries are now briefly described below.

Inflow Boundary

At the inflow, the axial profiles of the primary stream (u-velocity) are either obtained from experimental data or are calculated for the particular Reynolds number. The axial component of secondary velocities were also similarly prescribed. No data were available for the radial component of the velocity and hence the v-velocity was set to be equal to zero at the inlet.

The turbulence intensity k, was specified by referring to experimental data, wherever available. Otherwise it was set to a small value as shown in Eq. (3.5).

Since there is no direct way of knowing the ε values, they were specified by following standard practices (such as Stephenson[30]). In the present study the k and ε values at the inlet were obtained by using the following relation

$$K_i = 0.05U_s^2 \qquad \epsilon_i = \frac{k_i^{3/2}}{0.5l}; \tag{3.5}$$

Where l is the characteristic length, it is taken to be equal to the diameter of the pipe.

Outflow Boundary

There is no unique definition of an outflow boundary. The procedure adopted here, and one which has found to work satisfactorily (e.g., Patankar[24], Mahmud et al.[21]) is to set to zero the gradients of all the dependent variables in the outflow direction. Hence the boundary conditions at the outflow are

$$\frac{\partial u}{\partial x} = 0 \qquad \frac{\partial v}{\partial x} = 0 \qquad etc.$$

It should be noted that for the particular geometry considered in this study, prescription of zero gradient is truly valid at the distance where the flow has reached a situation when it can be called as fully developed. However, this would need a large number of grids in the x-direction and hence is not practically

feasible. The concern in the present study is to see the flow development pattern only in the initial region. So although the outflow boundary is placed at a distance x = 60 r_t the results of computation are reported only upto $x/r_t = 20$. It has been checked that the upstream effect of zero gradient boundary condition did not transmit upto $x/r_t = 20$.

Axis of Summetry

It can be clearly seen from Fig. 3.1, that there is an axis of symmetry in the flow domain. Hence, for all the computations at the axis (i.e., r = 0), the following boundary conditions were applied.

$$\frac{\partial u}{\partial r} = \frac{\partial k}{\partial r} = \frac{\partial \epsilon}{\partial r} = 0$$

and the radial component v = 0.

Solid Wall

No slip boundary conditions were applied for the velocity components. That is u = v = 0 at the solid wall.

For the turbulence quantities, the wall function (Launder and Spalding[19]) approach was followed. This method eliminates the need for putting large number of grids near the wall for the resolution of a small boundary layer near the wall and employs the log-law of the wall. This is a widely employed

technique and is also used in the current solution method. The detailed technique can be found in many references such as (Launder[19], Peric[25])

3.5 Closure

The governing equations for the particular fluid flow problem are presented in this chapter in a form which was used in the computer programme. The methodology of how the numerical calculations were carried out for one radian section of the solution domain are also presented in this chapter.

It has been mentioned earlier that the boundary conditions for every problem is a different one. Hence after incorporating the boundary conditions into the available computer programme, the code was first tested against some benchmark experimental and analytical results. Then the tested programme was used for the present study. In the next chapter these aspects along with the results and discussions are presented.

CHAPTER - IV

RESULTS AND DISCUSSIONS

4.1 Introduction

This chapter presents the analysis of the results obtained from the numerical prediction of coaxial axisymmetric confined jet in the developing region. Test results for the validity of the programme along with comparisons with other authors (viz., Razinsky[27] and Hasan[11]) are also presented in this chapter. Mean velocities, radial velocities, turbulence intensities and pressure distribution in the axial direction are analysed to produce information regarding the characteristics of coaxial confined jet. Comments on the results of the present investigation are also given in this chapter.

The investigation was carried out for four different inlet velocity profiles with constant velocity ratio $U_s/U_p = 0.023$ (Fig. 4.3a-b) and five different velocity ratios viz., 0.023, 0.05, 0.1, 0.2 and 0.5 at Reynolds number (defined in chapter 1) of 3.28 X 10^4. To investigate the effect of Reynolds number plug velocity profile and a standard 1/7th power law profile at Reynold number of 3.28 X 10^5 and velocity ratio of 0.5 are also considered. All these investigation were carried out with constant radius ratio $r_t/r_n = 2.48$, because experimental results were available with this radius ratio. All the computations were done on 80386 (ACER,System-15) computer situated in the Mechanical Engineering Department of BUET. Now the results obtained for different cases will be discussed in the following sections.

4.2 Testing of Computer Programme

Before using the available computer code to this study of coflowing confined jet, sufficient tests were carried out by solving a variety of flow in which code performance could be assessed. During testing of the code, preference was given to laminar flows to avoid complications due to uncertainities of turbulence model but turbulent flow case was also included to allow comparison with the results of other authors and to ensure that the code is functioning for k-ε model. Laminar flows considered in this work are the developing flows through circular pipe and parallel plate for Reynolds number of 160. Computations were done on a 40 X 25 grid (40 in the axial direction and 25 in the radial direction). The flow was allowed to develop from a plug inlet profile and at 60 diameters downstream, the flow was found to reach fully developed state and the axial velocity $(U/\overline{U})$ is compared with the analytical results of Schlichting[29]. The comparison for the circular pipe is shown in Fig. 4.1a. It can be seen that the computed data fully match with analytical results.

Next, for the same flow configuration, a developing turbulent flow through a circular pipe was studied. For a Reynolds number of 1.6×10^4 and at 60 diameters downstream from the inlet, the computed velocity $(U/\overline{U})$ (Fig.4.1b) is compared with the experimental data available in Schichting[29]. In this case also, the comparisons are good except near the wall where the computed results are lower

than the experimental data. This may be due to insufficient grid refinement near the wall and also the experimental results in this zone may not be that accurate as elsewhere.

These two test cases ensure that the boundary conditions like zero-gradient at outlet, axis of symmetry, and wall function (see § 3.4) are properly incorporated into the programme. Finally, the experimental investigation of Razinsky et al.[27] on coflowing confined jet was simulated by this code. In this case, radius ratio (r_t/r_n) was 3.0 which is different from others. This test case is given at the end of the chapter along with other relevant discussion (§ 4.9).

4.3 Selection of Grid and Convergence

The computations are based on grid pattern 70 X 40 (70 in the x-direction and 40 in the r-direction) as shown in Fig. 4.2. After computations with other grids such as 40 X 25, this final grid is selected. The final grid is found to yield almost grid independent results.

The computer programme used Upwind differencing scheme of Patankar[24] in all the computations. Another convection scheme, called Quick, (Leonard[20]) was also available in the programme but due to some oscillations it was not tried. However, as outlined in Chapter 5, computations with higher order schemes is left for future as the time it takes to establish it reliability was beyond the scope of this thesis.

Typically 600 iterations were required for a complete convergence (§ 3.3) and the time required per iteration was about 10 secs. It is observed that, for higher velocity ratios, the convergence is faster.

In the following sections, the results of various problems for different inlet parameters are presented.

4.4 Mean Axial Velocity

The mean axial velocities at the downstream of the jet for four different inlet velocity profiles are shown in Figs. 4.4a to 4.4d and for different velocity ratios are shown in Figs. 4.5a to 4.5d. The mean velocities at Reynolds number of 3.28×10^5 for plug inlet profile and 1/7th power law profile at velocity ratio of 0.5 are presented in Figs. 4.6a and 4.6b. For convenience of presentation, the velocity profiles are drawn at eight axial locations (X = 0, 0.4, 1.4, 3.0, 5.7, 7.25, 9.25 and 16.0).

It can be seen from Figs. 4.4a to 4.4d that the primary core flow evidenced by a section of axial velocity profile near the centre line (i.e., $r/r_t = 0.0$) having constant U, exists between X = 1.4 and 3.0 for profiles 1 and 2, whereas for profiles 3 and 4 it is almost non-existent. On the other hand, the secondary stream core flow can be observed only for the first axial location i.e., X = 0.4. This is due to the fact that U_s/U_p is very small and hence the secondary core is very quickly consumed.

The other characteristic feature is the presence of negative velocity near the wall ($r/r_t = 1.0$). For inlet profile-1 (Fig. 4.3a), this negative velocity is seen to exist at all the axial locations after X = 0.4 whereas for other three inlet profiles of Fig. 4.3a - 4.3b (Profiles 2, 3, 4) there are two negative velocity zones.

The first recirculation zone for profiles 2, 3 and 4 is seen to exist in the range, $1.4 < X < 7.25$. The second recirculation is seen at X = 16.0, 9.25 and 7.25 for inlet profiles of 2, 3 and 4 respectively.

The exact length of the first recirculation and the exact location of the beginning of second recirculation are given in Table 4.1.

Table 4.1: Location and Length of recirculation Regions

Inlet Profile	Displace-ment Thickness δ^*	Beginning of first Recircula-tion	End of first Recircula-tion	Length of first Recircula-tion	Beginning of second Recircula-tion
2(Fig.4.3a)	.0068	X = 1.15	X = 6.25	X = 5.1	X = 10.16
3(Fig.4.3b)	.0315	X = 1.44	X = 6.16	X = 4.72	X = 8.36
4(Fig.4.3b)	.0325	X = 2.2	X = 5.5	X = 3.3	X = 6.63

It can be concluded from the above table that the beginning and ending of the first recirculation follows a distinct order with displacement thickness. For smaller δ^*, the recirculation starts earlier in the duct and is consumed at further downstream. Fig. 4.4e shows the contour plot of stream function for profile-2.

Although the first recirculation was also observed in the experimental measurements of Hasan[11] * the second recirculation was not reported by him. However, Rajaratnam[26] refers to such a recirculation. The second recirculation was seen to exist at X $\cong$ 30 and since the present investigation is limited in the early regions at X $\simeq$ 20, this is not reported here.

It is observed from the plots of Fig. 4.4a and 4.5d that recirculation is present only for the lowest velocity ratio, $U_s/U_p = 0.023$. No recirculation was observed for other velocity ratios. This finding supports the findings of Champagne and Wygnanski[5] in which they studied the coaxial confined jet for velocity ratios of 0.1, 0.2, 2 and no recirculation was observed. The reason for the recirculation at the lowest velocity ratio is that the phenomenon is very similar to a sudden expansion associated with an adverse pressure gradient, as shown in Fig. 4.15 From Figs. 4.5d and 4.6a it is easily seen that for higher Reynolds number the rate of development of axial velocity is quicker than the lower Reynolds number. The existence of a `kink' near the junction between the secondary and primary streams can be observed upto X = 5.7. This may have an effect in the turbulence intensity distribution as seen in Fig. 4.9a - d. Inlet velocity profiles also affect the

---

* Comparison of the predictions with those of Hasan11 will be presented in § 4.9.

development of flow. From Figs. 4.6a and 4.6b it is evident that for 1/7th power law inlet profile, development rate is quicker than plug inlet velocity profile. This is because, for 1/7th power law profile, the existence of shear layer enhances rapid mixing.

4.4a Radial Velocity

For the flow configurations considered, the variation of V-velocity are very similar. Initially, at X = 0, its value is set to be equal to zero. Maximum magnitude of the radial velocity is obtained within X = 1 to 3. Then it decreases to a very low value and becomes constant along the radial direction. Fig. 4.7 shows the V-velocity profile for plug velocity inlet and Re = 3.28 X 10^4. It can be seen that the maximum value of V is approximately 7% of U_e at X = 1.4. The radial location for maximum is found to be within the shear layer of the primary jet.

4.5 Turbulence Intensities

Turbulence intensities defined as $U' = \sqrt{2k/3}$ at different downstream locations for four inlet profiles are shown in Figs. 4.8a-d, and for different velocity ratios are shown in figs. 4.9a-d. Turbulence intensities at the high Reynolds number of 3.28 X 10^5 are shown in Figs. 4.10a and 4.10b. From plots in Figs. 4.8a-d, it is seen that

in the initial region the intensity curves have two maximum (curves C and D in Figs. 4.8b-d) which indicate two mixing regions as discussed in § 4.4. Existance of such two discrete mixing regions is also reported by Champagne and Wygnanski[5] and Razinsky et al[27]. After complete disappearance of two discrete mixing regions, turbulence intensity variation is reduced and the peak of the profile is generally shifted towards the axis of symmetry. This shifting is clearly seen in Fig. 4.8d for profile 4. It is further observed from Fig. 4.8b-d that maximum intensities occur for profile 4 (largest δ^*) and is equal to 18% of U_c at an axial location of X = 16.0. Turbulence intensity for prrofile 1 (Fig. 4.8a) is somewhat different. It can be seen that starting at X = 3.0, there is little difference in the turbulence intensity and the maximum value is 28% of U_c. This is possibly due to the largest velocity gradient at primary-secondary junction associated with plug profile. Figures 4.9a-d reveal that with increase of velocity ratio the magnitude of normalised turbulence intensity is lower. On the other hand, as the secondary stream velocity increases, turbulence intensities near the wall also increases. The reason can again be attributed to the larger gradients of velocity at higher values of U_s/U_p.

At the high Reynolds number of 3.28 X 10^5 (Figs. 4.10a-b), the magnitude of turbulence intensity increases rapidly in the initial region and after X = 5.7 it is almost constant in the region near the axis of symmetry. On the other hand, an increasing trend is observed near the wall which is obviously due to the developing boundary layer at the wall. Variation of turbulence intensities along the middle

of the wall and the axis of symmetry (i.e., along $r/r_t = 0.5$)** for four inlet velocity profiles are shown in Fig. 4.11. The variation shows that turbulence intensity increases quickly for plug profile (Profile-1) and becomes constant earlier than other cases. For the other inlet profiles, the increasing trend is a two-stepped curve being monotonous in the latter half.

Figure 4.12 shows the turbulence intensity variations along $r/r_t = 0.5$ for different velocity ratios. All the curves exhibit similar pattern and are made up of three distinct regions. The first part is a curve having constant magnitude of intensity, the second part represents a sharp rise and the third again is a portion of constant turbulence intensity. Interestingly, the axial location of the beginning of the second part of the curve is observed to increase with increase of velocity ratio (i.e., for $U_s/U_p = 0.023$ and 0.5, the sharp rise occurs at X = 1.5 and 6.0 respectively). The results also demonstrate that higher velocity ratio suppresses turbulence intensity. Figure 4.13 shows the variation of turbulence intensity along $r/r_t = 0.5$ at Reynolds number of 3.28×10^5 for plug profile and 1/7th power law profile. Both the curves show the same nature but for plug profile turbulence intensity increases earlier than 1/7th power law profile. In both cases the turbulence intensities become almost constant nearly at X = 4 to 5.

** This variation may be of particular significance for certain applications such as a furnace. The reason is that the maximum turbulence intensity occurs near this zone and hence the burning of fuel also takes place in this area.

4.6 Static Pressure Variation

Static pressure variations for different inlet profiles and different velocity ratios are shown in Figs. 4.14 and 4.15. Figure 4.14 indicates that for different inlet profiles the static pressure variation are similar i.e., first increase and then become constant. This nature was also found by Hasan[11] . From Fig. 4.15 it can be observed that as the velocity ratio increases the pressure becomes constant earlier in the mixing pipe. It is found that although the pressure is seen to be constant for $U_s/U_p = 0.5$ at and after X = 1.5, it is not so for other cases, which show an adverse pressure gradient.

Razinsky[27] pointed out that for lower velocity ratios the axial pressure distribution increased in the mixing region and for higher velocity ratios the pressure gradients became favourable. The variations of pressure distribution thus agree with those of Razinsky[27]. Fig. 4.16 shows the variation of pressure for plug and 1/7th power law profile for Reynolds number 3.28×10^5. This figure also demonstrates similar nature.

4.7 Variation of Half Radius ($R_{1/2}$)

For different inlet velocity profiles half radius $R_{1/2}$ i.e., radius at which $(U-U_s) = 0.5\ (U_c-U_s)$ at different axial locations along the downstream are drawn. This is plotted (Fig. 4.17) in order to show the growth rate of the jet. It can be seen that the jet is spreading in the early region of the mixing pipe and after that it shows a monotonic downward behaviour. This findings is different from that of Hasan[11], where he has demonstrated a monotonic rising trend. The difference is probably due to the shortcoming of the turbulence model, as it will be discussed in § 4.9 (and also reported by Mahmud et al.[21]) that the axial velocities are usually underpredicted at further downstream location.

4.8 Excess Velocity Profile

An excess velocity profile $[(U-U_s)/(U_c-U_s)$ vs. $r/r_{1/2}]$ for the inlet profile-2 at axial distances of X = 2.7, 4.5, 6.65, 7.85 and 9.5 is drawn in Fig. 4.18. All the plots follow the nature of empirical equation proposed by Hill[13]. From this plot it is also clear that matching with the empirical equation is better for higher values of X i.e., at further downstream. This shows the correct behaviour of the jet because Hill's equation is based on a large number of data collected for the developed velocity profiles.

4.9 Comparison with Experimental Result

The flow configurations for inlet profiles 2, 3 and 4 at Re = 3.28 X 10^4 (radius ratio = 2.48) are compared with the experimental data of Hasan[11]. The comparisons are shown in Fig. 4.19a-c. The qualitative nature has been computationally reproduced for all the curves. However, some discrepancies are present which may be due to inappropriate turbulence model as mentioned by Mahmud, et al[21]. Apart from this, there were some uncertainties in the experimental measurement as mentioned by Hasan[11] and also due to the fact that inlet values of turbulence intenisty was not measured. Further there may be some difference due to the reason that the present work considers the secondary stream to be forced-flow, whereas the experiment was conducted for induced flow.

Fig. 4.20 represents the comparison with experimental data of Razinsky, et. al[27]. The radius ratio (r_t/r_n) for this case is 3.0 and velocity ratio is equal to 0.33. The initial conditions are the same as that of the experiment. The comparison of U-velocity is shown in Fig. 4.20. The agreement is found to be quite reasonable. However, peaks and troughs are not properly reproduced which may be due to the deficiency of the convection scheme of Patankar[24]. As mentioned in Chapter 5, the application of a higher order scheme is expected to improve this prediction.

4.10 Closure

The results of the present investigation are presented and discussed in this chapter. The mean velocity, turbulence intensity, rate of growth of jet, static pressure, etc., are discussed in order to understand the flow pattern in the developing region of the confined jet. The findings are also compared with available experimental and analytical data, wherever available, in order to validate and also to highlight the shortcomings of the present work. In the next chapter the findings of the present thesis are summarized.Some proposals for improvement of the present results and also some new ideas are included.

CHAPTER V

CONCLUSIONS AND SUGGESTIONS FOR FUTURE WORK

In this chapter, a summary of what has been accomplished in the present work is highlighted. Some suggestions for future work are also given.

5.1 Findings of the Present Work

The study of flow in the developing region of an axisymmetric confined jet revealed both expected and unexpected features. The study of mean velocity, radial velocity, recirculation phenomena, pressure variation and turbulence intensity distribution revealed some important and useful aspects of confined jet flow. These are now summarized below.

1. Recirculation of coflowing confined jet depends on the jet velocity ratio U_s/U_p and also on the boundary layer of the inlet velocity profile. For the range of velocity ratio considered in this study, recirculation takes place for the lowest velocity ratio of 0.023 and its length is found to decrease with increasing boundary layer thickness.

2. Turbulence intensities decrease with increase of velocity ratio. For higher velocity ratio, turbulence intensity near the wall increases. At higher Reynolds number turbulence intensities rapidly become constant although the magnitude increases.

3. Radial velocity is observed to be very small having maximum magnitude (of the order 7.0% of U_o) near the entrance over the range of X = 1 to 2.

4. Boundary layer of the initial profile has little effect on static pressure variation downstream but the velocity ratio has considerable influence on it. The axial distance for the static pressure to become steady is found to be increasing with decreasing velocity ratio.

5. The radius at which the velocity is half of the centre line velocity [$U-U_s = 0.5\ (U_c-U_s)$] increases with increasing boundary layer thickness.

5.2 Suggestions for the Future Work

In the light of the present work, suggestions for future work are grouped into two catagories as mentioned below.

A. For improving the predictions of the present work, the following works may be recommended.

1. It is mentioned earlier that some of the discrepancies in the predictions have possibly occurred due to the limitation of the turbulence model. Hence different turbulence models (Gibson et al[10]) may be investigated for better agreements with experiments.

2. A higher order differencing scheme such as QUICK of Leonard[20] may be used for more accurate predictions.

3. Smaller size of grids may be used in order to resolve the thin shear layers.

B. Some additional ideas:

1. As mentioned in literature-review, swirling coaxial jets are quite common in engineering practice. Hence the present analysis may be extended by including a third component of velocity in the computer code, thus making the governing system a quasi-3D system.

2. To improve predictions of Hasan[11] by simulating the induced flow. This can be done by extending the flow region or by incorporating pressure boundary conditions.

3. More experimental data are required for code assessment. Specially for the type of Reynolds number considered in this study, very few works has come to the notice of the author where the inlet boundary layer effect has been reported. This needs more experiments to be carried out in the developing region.

4. By including particle dispersion, the analysis may be extended further for the simulation of furnaces using pulverised coal.

REFERENCES:

1. Agrawal D.P., Singh S.N. & Malhotra R.C., "Influence of Confinement Geometry on Mixing Characteristics of Co-Axial Swirling Jets", Indian Journal of Technology, Vol. 29, pp. 599-604, 1991.

2. Azim M.A., "Numerical Computation for Velocity and Temperature Within the Axisymmetric Turbulent Jets in Moving Surrounding", M.Sc. Engineering (Mechanical) Thesis, Bangladesh University of Engineering and Technology, Dhaka, 1984.

3. Barchilon M. and Curtet R., " Some Details of the Structure of an Axisymmetric Confined Jet with Backflow", Fluids Engineering Conference, ASME, Paper, 64-FE-23, pp. 1-17, 1964.

4. Becker H.A. Hottel H.C. and Williams G.C., "Mixing and Flow in Ducted Turbulent Jets". Proc. 9th International Symposiym, Combustion, pp. 7-20, 1962.

5. Champagne F.H. and Wygnanski I.J., "An Experimental Investigation of Co-axial turbulent Jets", J. Heat Transfer, Vol. 14, pp. 1445-1464, 1971.

6. Curtet R. and Ricou, F.P., "On the Tendency to Self-Preservation in Axisymmetric Ducted Jets," Fluids Engineering Conference, ASME, Paper 64-FE-20, pp. 1-11, 1964.

7. Dealy J.M., "The Confined Circular Jet with Turbulent Source," Symp. Fully Separated Flows, ASME., pp. 84-91, 1964.

8. Durao D. & Whitelaw J.H, "Turbulent Mixing in the Developing Region of Co-axial Jets", Journal of Fluids Engineering, pp. 467-473, 1973.

9. Exley J. T. and Brighton J. A., "Flow Separation and Reattachment in Confined Jet Mixing", ASME, paper 70-FE-B, pp. 1-11, 1970.

10. Gibson M.M., Jones W.P., McGuirk J.J., Whitelaw J. H., "Lectures on Turbulence Models for Computational Fluid dynamics", Department of mechanical Engineering, Imperial College, London, 1988.

11. Hasan R.G.M., "A Study of Induced Flow Development Along the Downstream of an Axisymmetric Jet Issuing Axially into a Smooth Pipe", M.Sc. Engineering (Mechanical) Thesis, Bangladesh University of Engineering and Technology, Dhaka, 1985.

12. Hembold H.B. Luessen G. and Heinrich A.M., " An Experimental Investigation of Constant Pressure and Constant Diameter Jet Pumps", Engineering Report 147, University of Wichita, 1954.

13. Hill B.J., "Two-dimensional Analysis of Flow in Jet Pumps", ASCE, J. of Hydraulics Division, Vol. 99, No. HY 7, pp. 1009-1026, 1973.

14. Hill, P.G., "Turbulent Jets in Ducted Streams", Journal of Fluid Mechanics, Vol. 22, pp. 161-186, 1965.

15. Hinze J. O., Turbulence, McGraw-Hill, New York, 1950.

16. Jones W. P., Launder B. E., "The Prediction of Laminarisation with a Two-Equation Model of Turbulence", International Journal of Heat and Mass Transfer, Vol. 15, p. 301, 1972.

17. Ko N.W.M. and Lam K.M., "Flow Structures of Coaxial Jet of Mean Velocity Ratio 0.5", AIAA Journal, Vol. 27, No. 5, pp. 513-514, 1989.

18. Kwan A.S.H. & M. Ko N.W., "The Initial Region of Subsonic Co-Axial Jets", J. Fluid Mechanics, Vol. 82, Part-2, pp. 273-287, 1977.

19. Launder B. E., Spalding D. B., "The Numerical Computation of Turbulent Flows", Comp. meth. appl. Mech. and Engg., Vol. 3, p. 269, 1974.

20. Leonard, B.P., "A Stable and Accurate Convective Modelling Procedure Based on quardratic Upstream Interpolation", Comp. Meth. Appl. Mech. Engg., Vol. 19, pp. 59-98, 1979.

21. Mahmud T., Truelove J. S. and Wall T. F., "Flow Characteristics of Swirling Co-axial Jets from Divergent Nozzles", J. Fluids Engg., ASME, Trans., vol. 109, pp. 275-282, 1987.

22. Mikhail S., "Mixing of Co-axial Streams Inside a Closed Conduit", J. Mech. Engg. Science, Vol. 2, pp. 59-68, 1960.

23. Morton B. R., "Co-axial turbulent Jets", Int. J. Heat Mass Transfer 5, pp. 955-965, 1962.

24. Patankar S.V., Numerical Heat Transfer and Fluid Flow, McGraw-Hill, New York, 1980.

25. Peric H., "A Finite Volume Method for the Prediction of Three-dimensional Fluid Flow in Computer Duct", Ph.D. Thesis, University of London, 1985.

26. Rajaratnam N., Development in Water Science 5, Turbulent Jets, 1976.

27. Razinsky E. & Brighton J. A., "Confined Jet Mixing for Non-separating Conditions", Journal of Basic Engineering, pp. 333-349, 1971.

28 Roache P. T., Computational Fluid Dynamics, Hermosa Publishers, Albuquerque, New Mexico, 1976.

29. Schlichting H., Boundary layer Theory, McGraw-Hill Book Company, New York, 1979.

30. Stephenson P.L., "A Theoretical Study of Heat Transfer in Two-dimensional Turbulent Flow in a Circular Pipe and between Parallel and Diverging Plates", Int. J. of Heat Mass Transfer, Vol. 19, pp. 413-423, Pergamon Press, 1976.

31. Tennekes H., Lumley J. L., A First Course in Turbulence, MIT Pressm 1985.

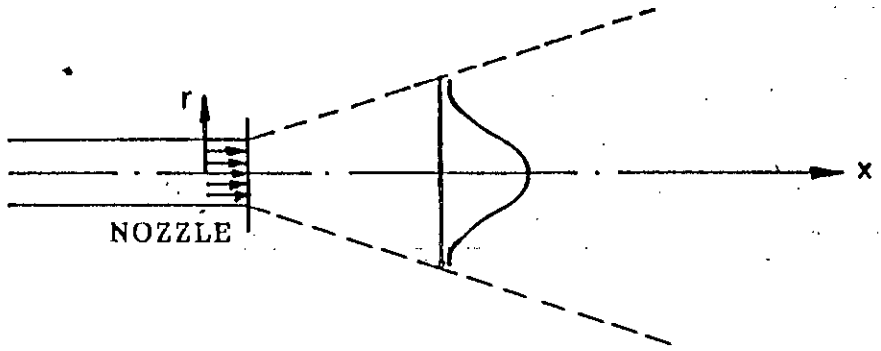

FIG 1.1a FREE JET

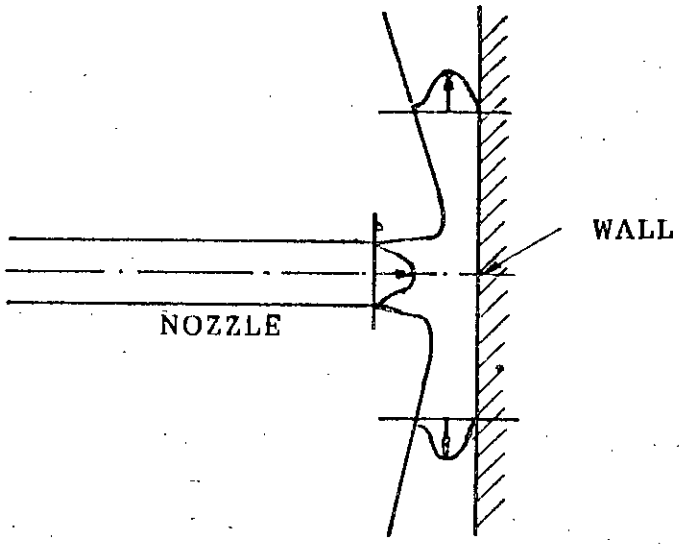

FIG: 1.1b WALL JET

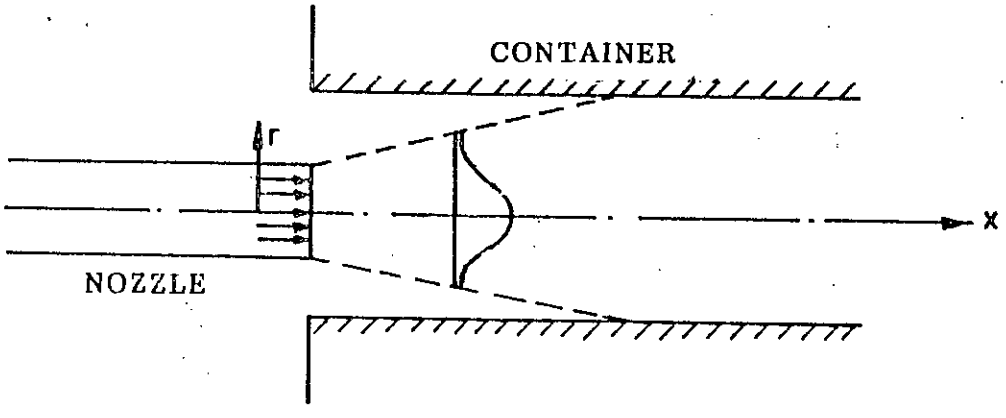

FIG:1.1c CONFINED JET

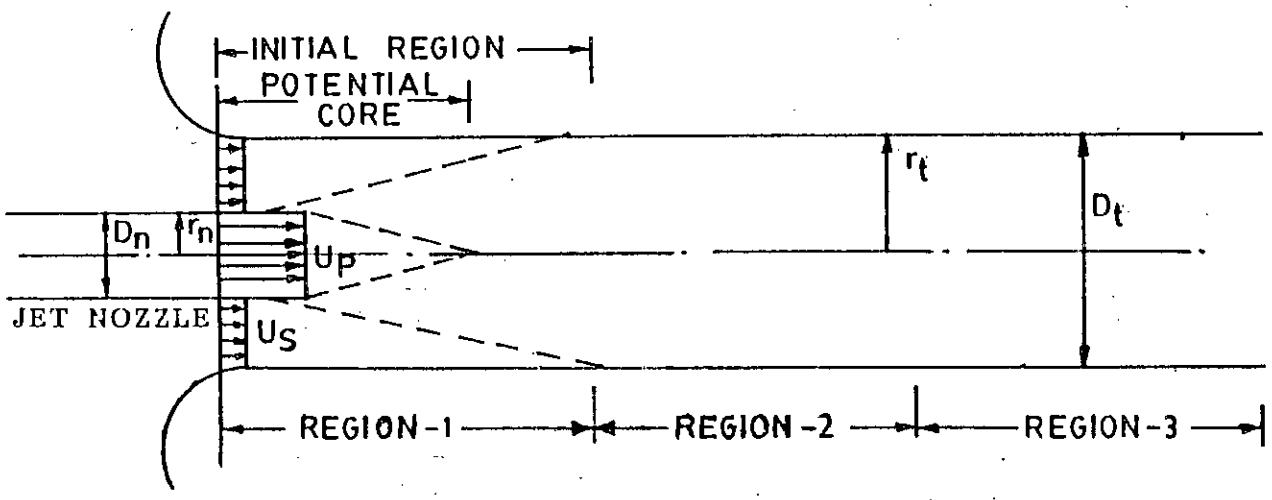

FIG:1.2 SCHEMATIC DIAGRAM OF COAXIAL CONFINED JET

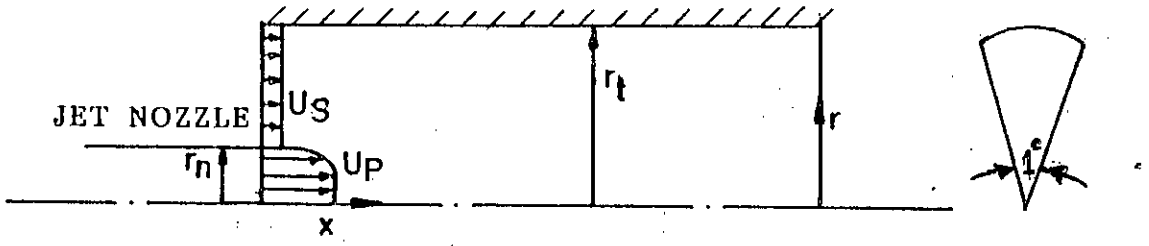

FIG:3.1 CO-ORDINATE SYSTEM AND BOUNDARIES

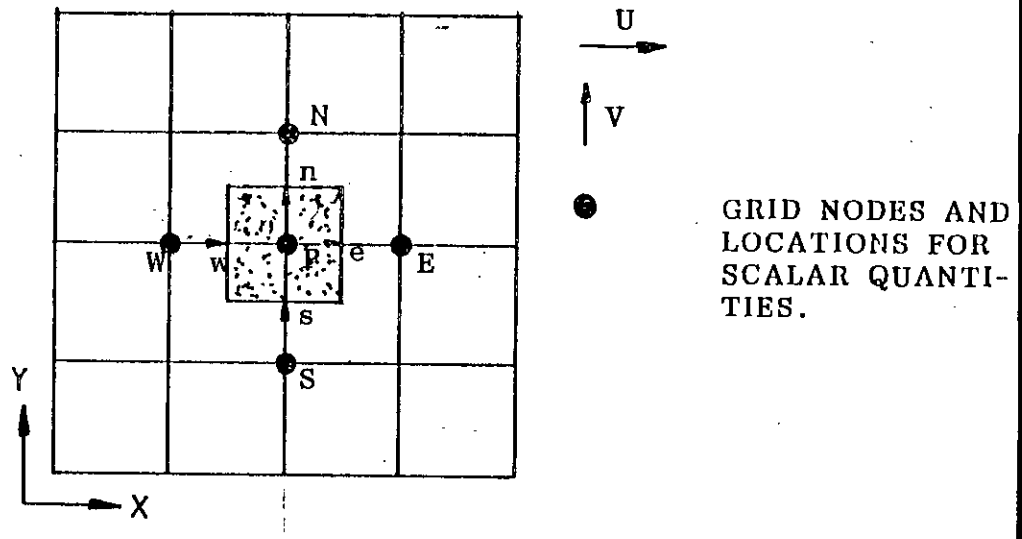

FIG: 3.2 A TYPICAL CONTROL VOLUME AND LOCATION OF DIFFERENT FLOW VARIABLES

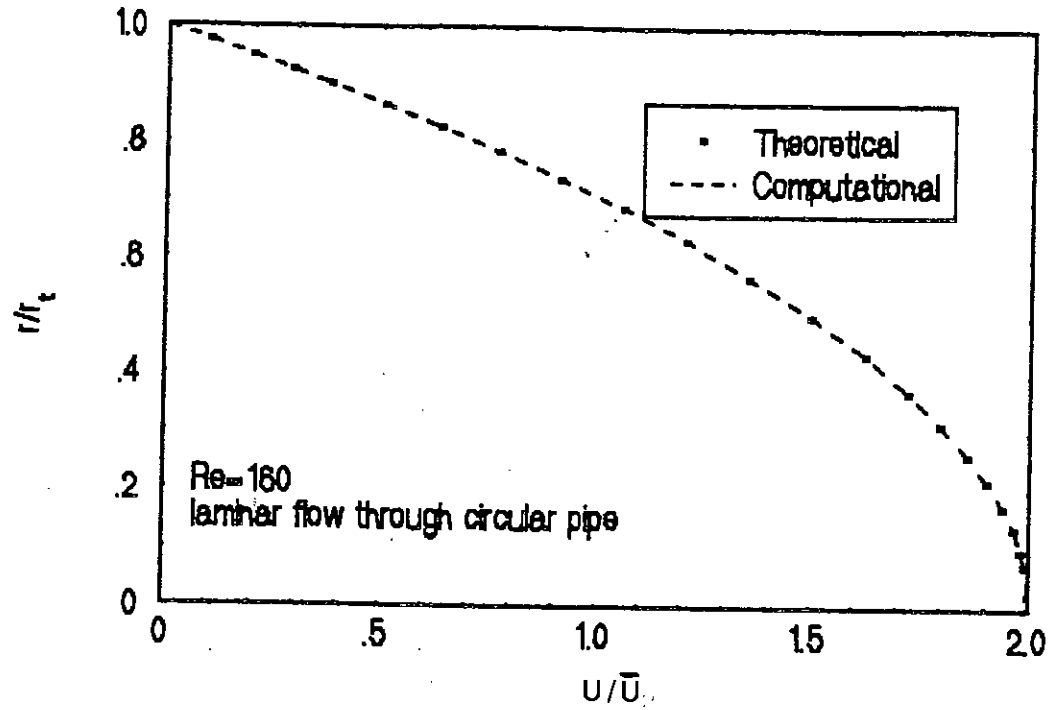

FIG:4.1a COMPARISON OF CODE WITH THEORETICAL FOR LAMINAR FLOW THROUGH CIRCULAR PIPE

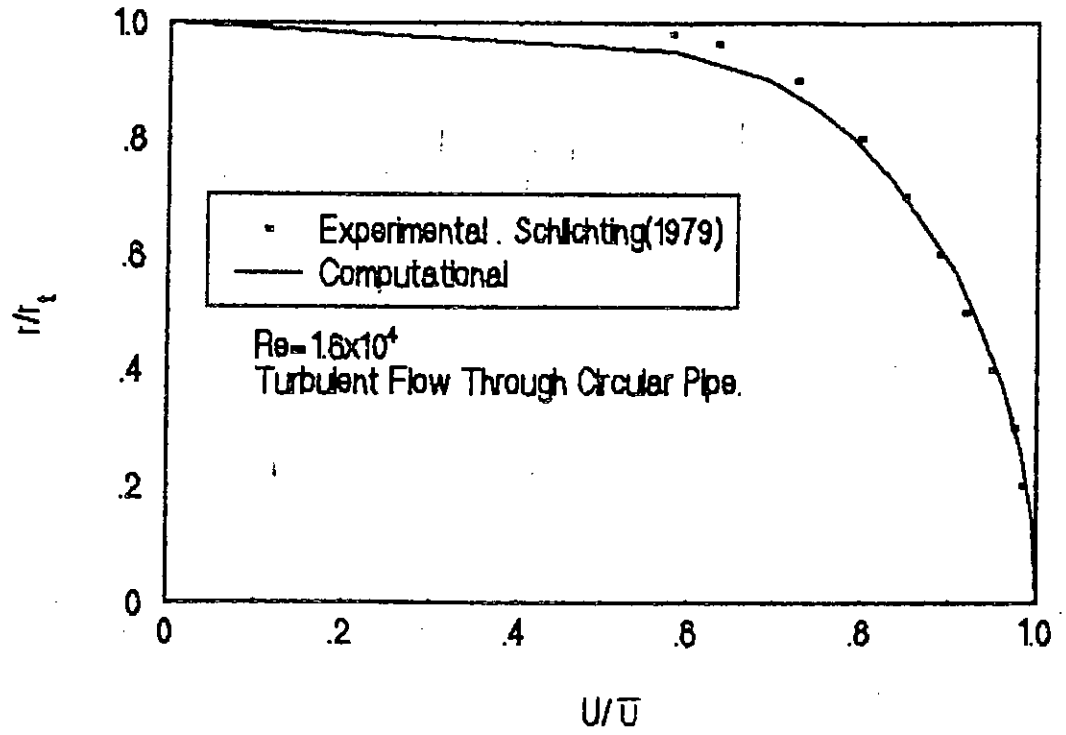

FIG: 4.1b COMPARISON OF CODE WITH EXPERIMENT FOR TURBULENT FLOW THROUGH CIRCULAR PIPE

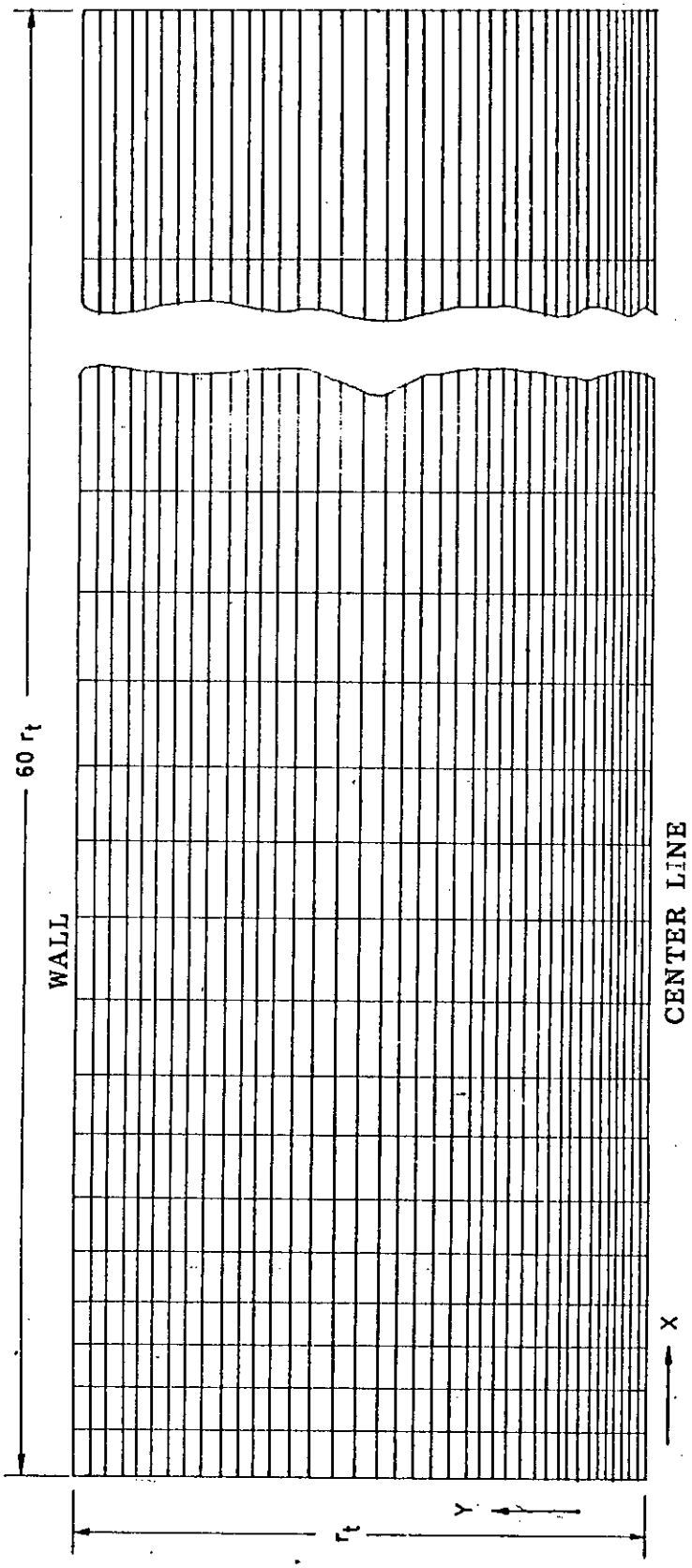

FIG: 4.2 GRID USED FOR COMPUTATIONS(70x40)

PROFILE-1

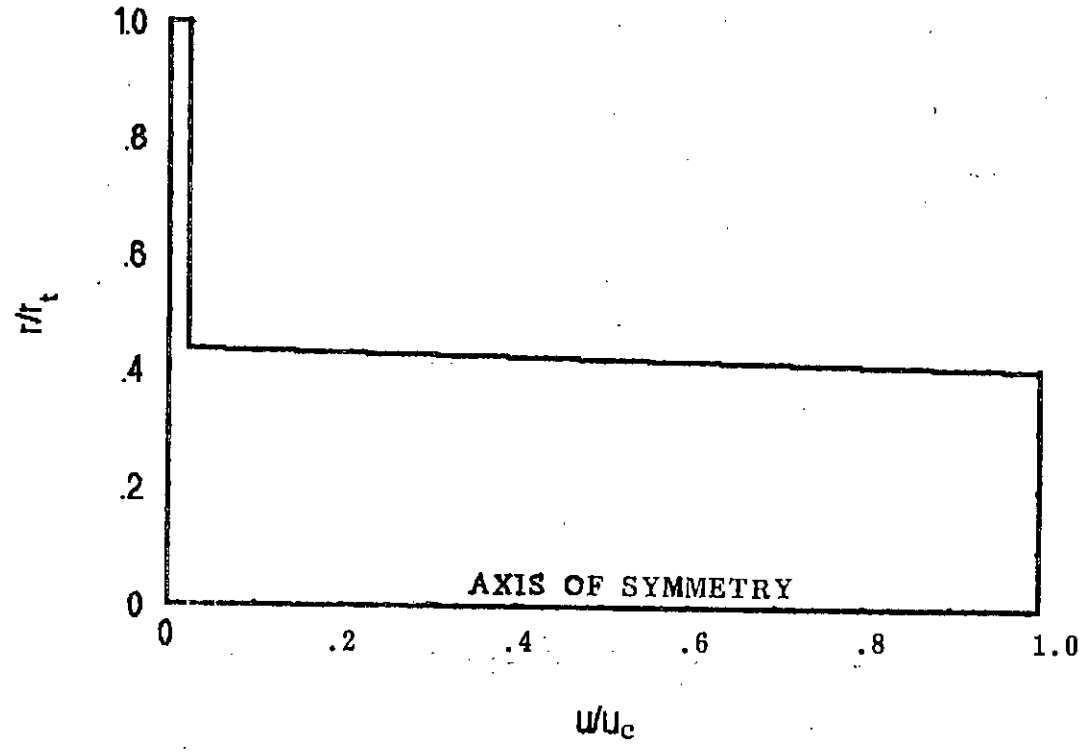

PROFILE-2

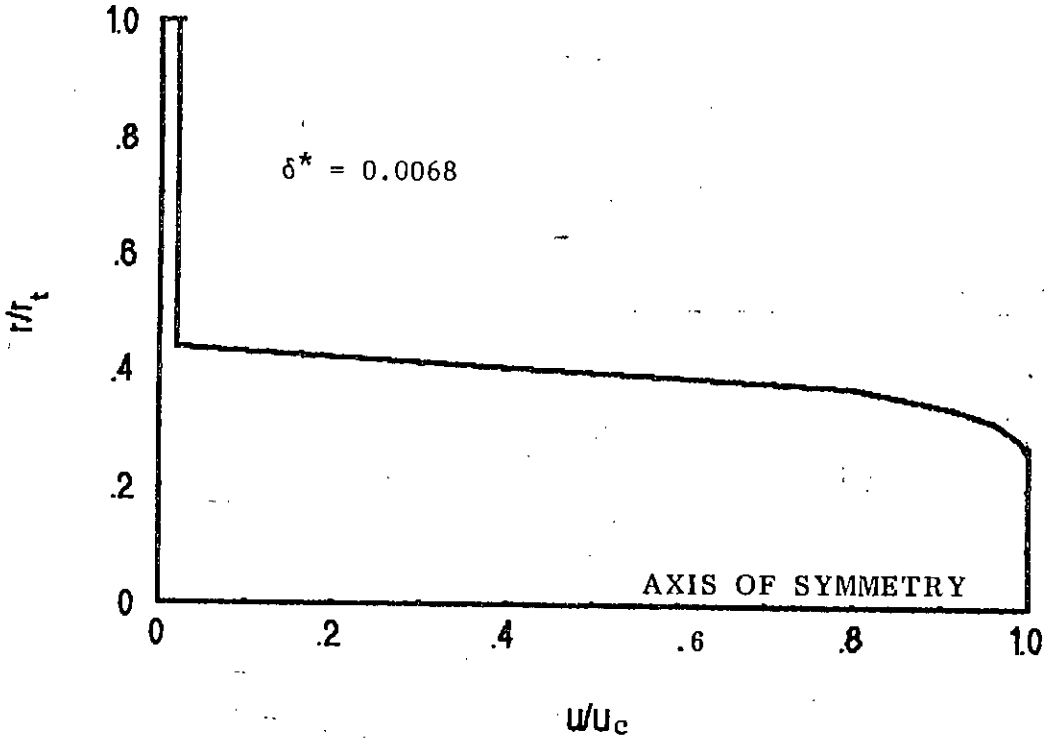

FIG: 4.3a -INLET VELOCITY PROFILES

PROFILE-3

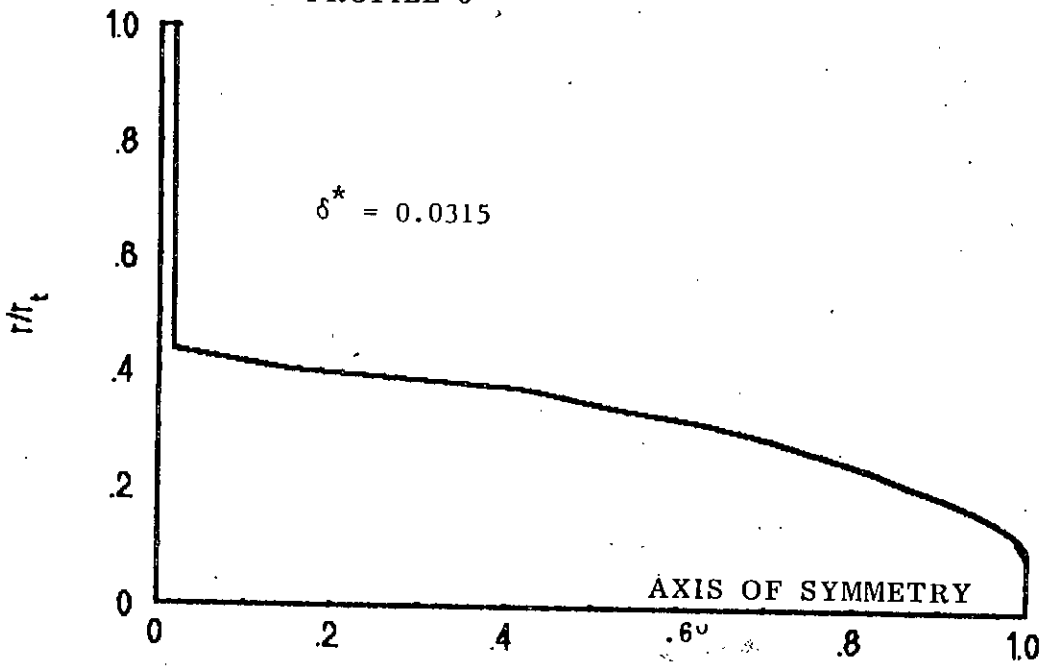

PROFILE-4

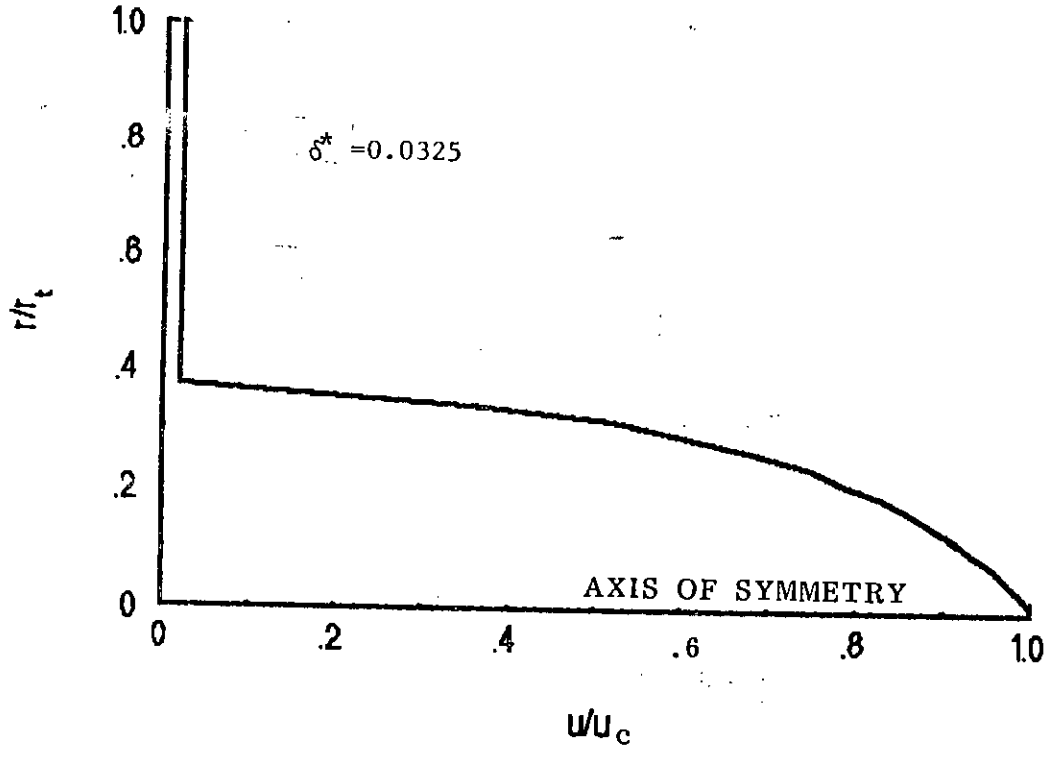

FIG:4.3b (Continued) INLET VELOCITY PROFILES

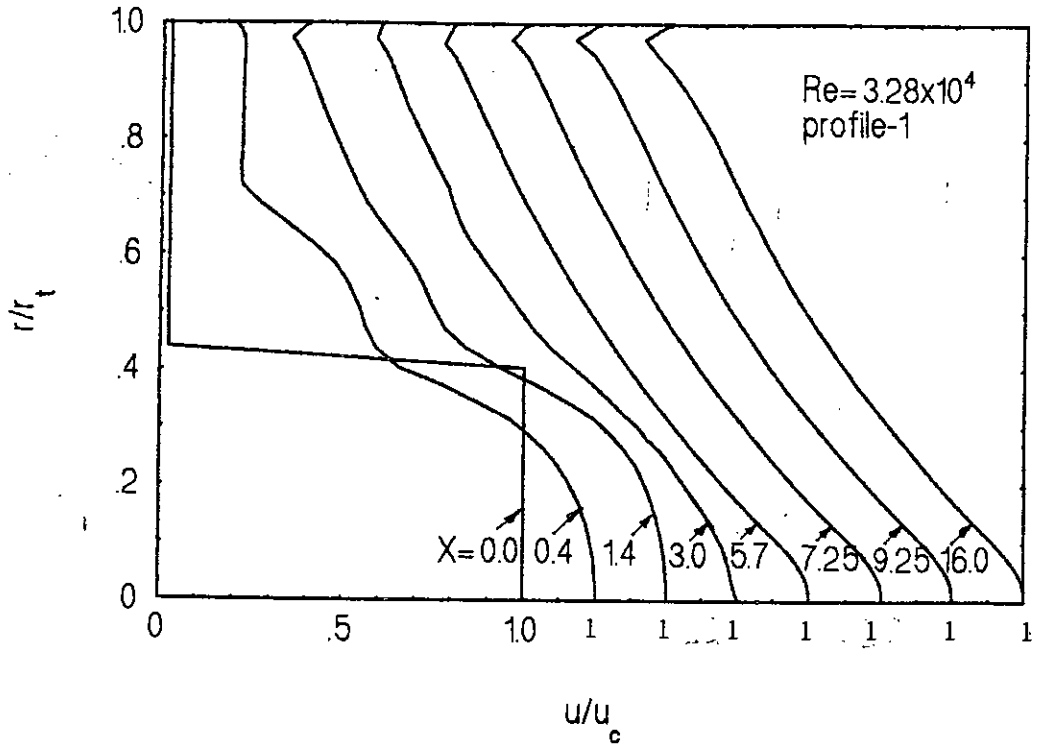

FIG: 4.4a MEAN AXIAL VELOCITY (U/U_c) AT DIFFERENT AXIAL LOCATIONS FOR INLET PROFILE-1

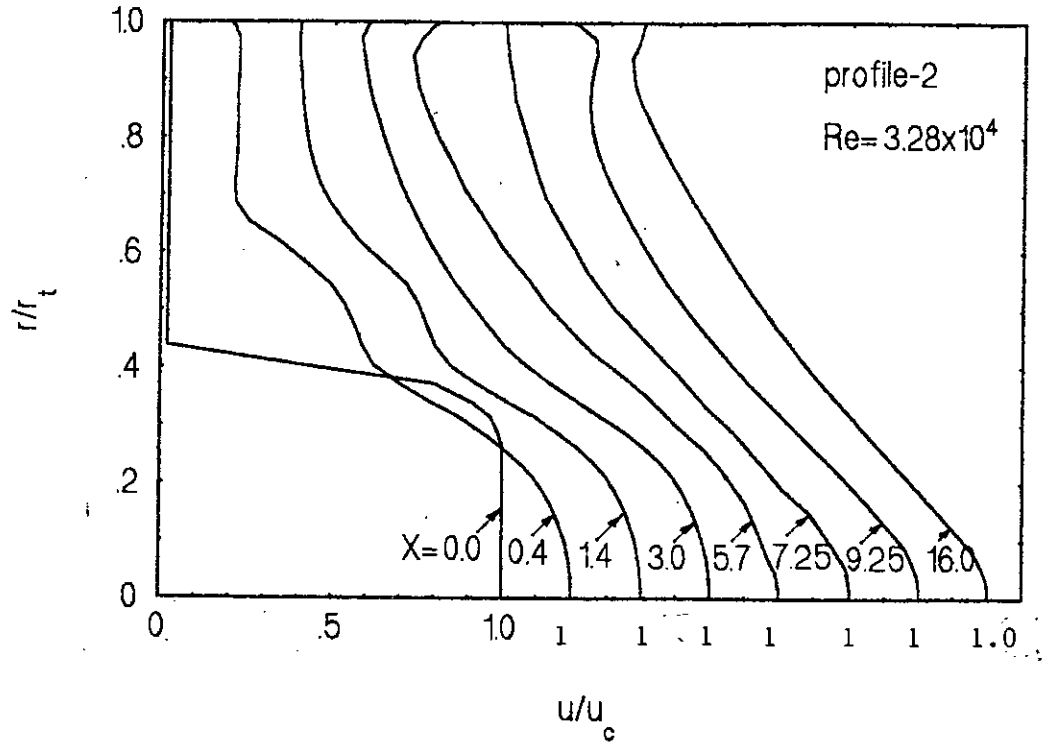

FIG 4.4b MEAN AXIAL VELOCITY(U/U_c) AT DIFFERENT AXIAL LOCATIONS FOR INLET PROFILE-2

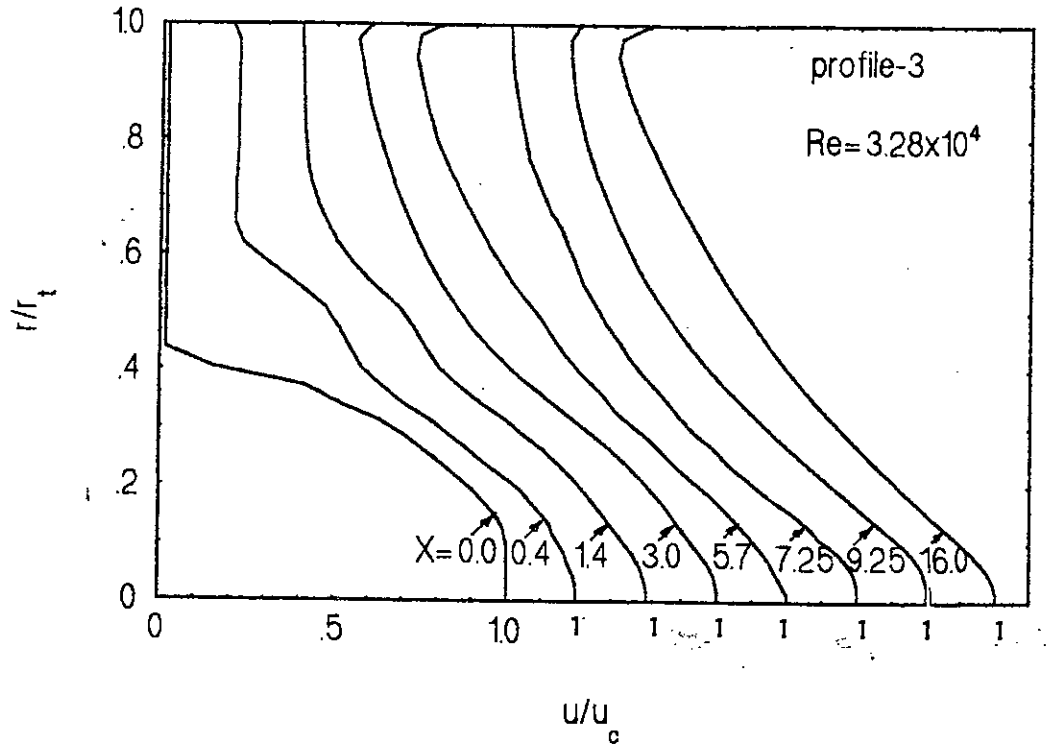

FIG:4.4c MEAN AXIAL VELOCITY(U/U_c) AT DIFFERENT AXIAL LOCATIONS FOR INLET PROFILE-3

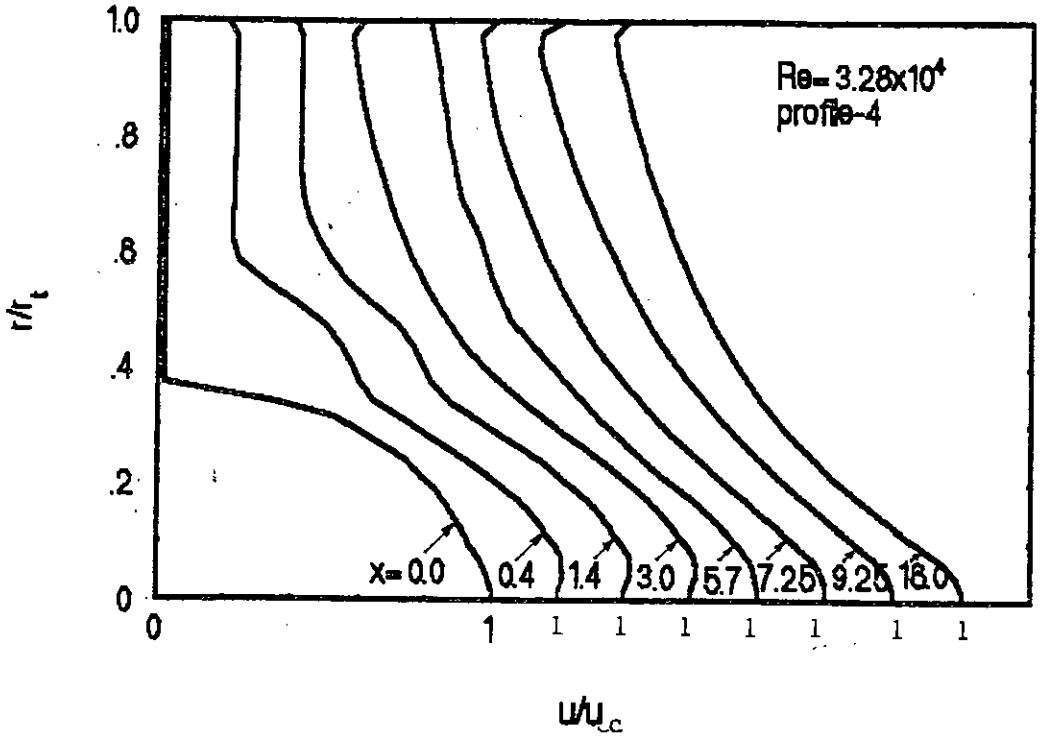

FIG: 4.4d MEAN AXIAL VELOCITY(U/U_c)AT DIFFERENT AXIAL LOCATIONS FOR INLET PROFILE-4

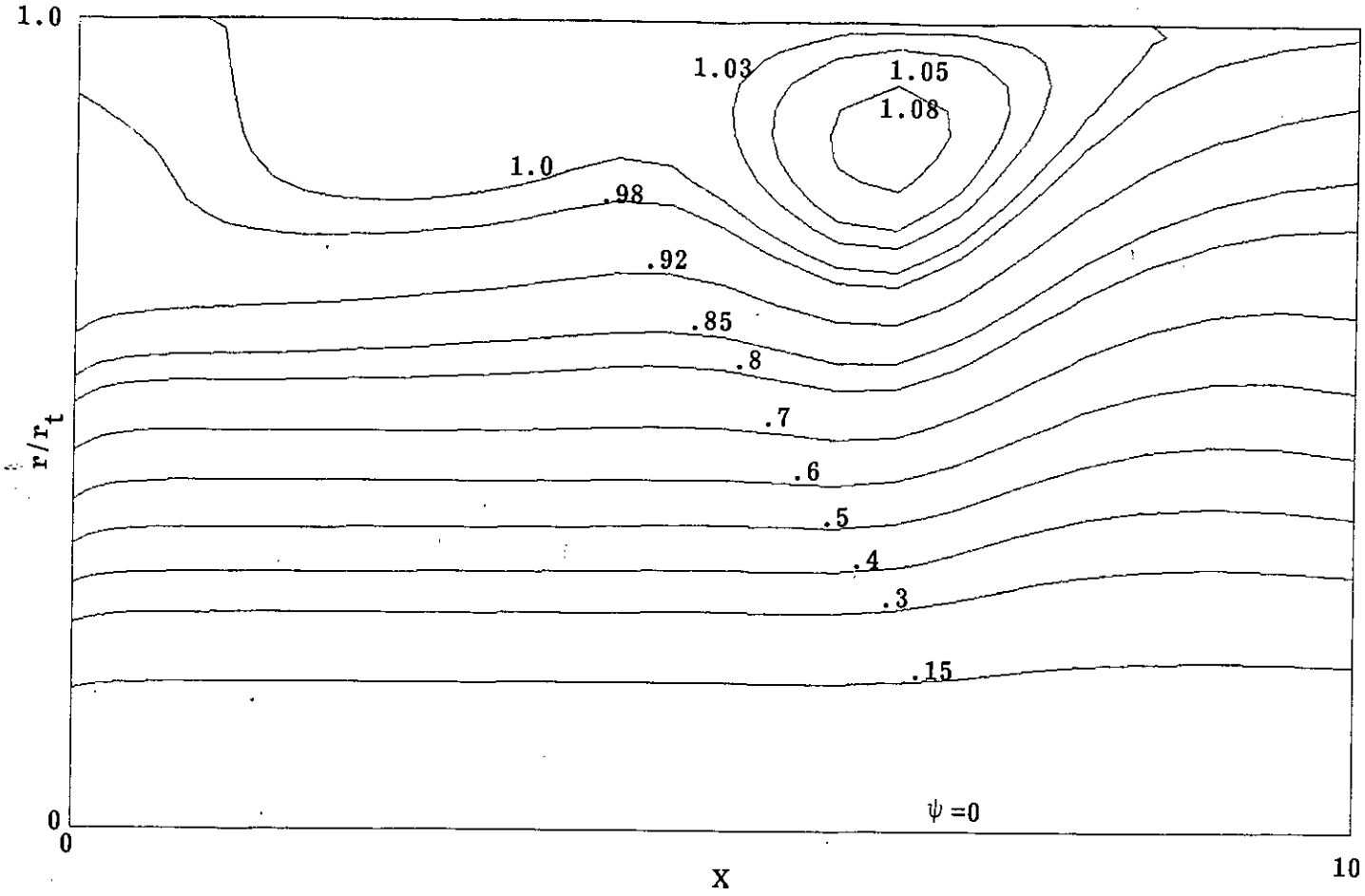

FIG: 4.4e CONTOUR PLOT OF STREAM FUNCTION FOR PROFILE-2(X=0--10)

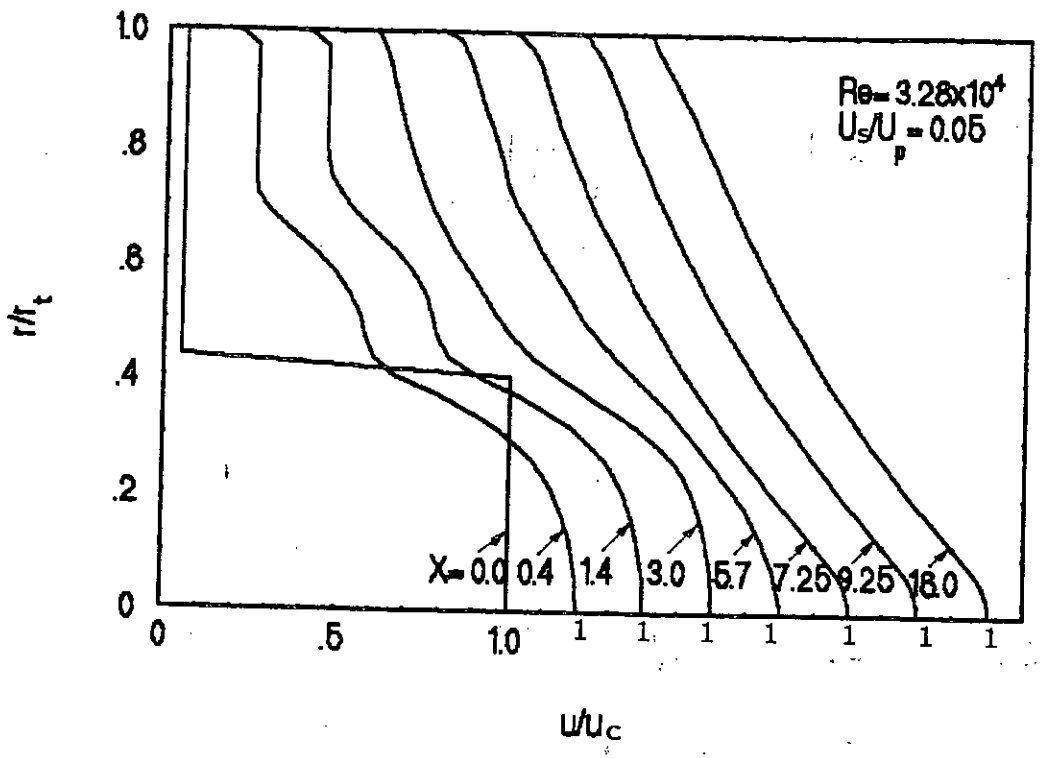

FIG:4.5a MEAN AXIAL VELOCITY(U/U_c) AT DIFFERENT AXIAL LOCATIONS FOR U_s/U_p=0.05

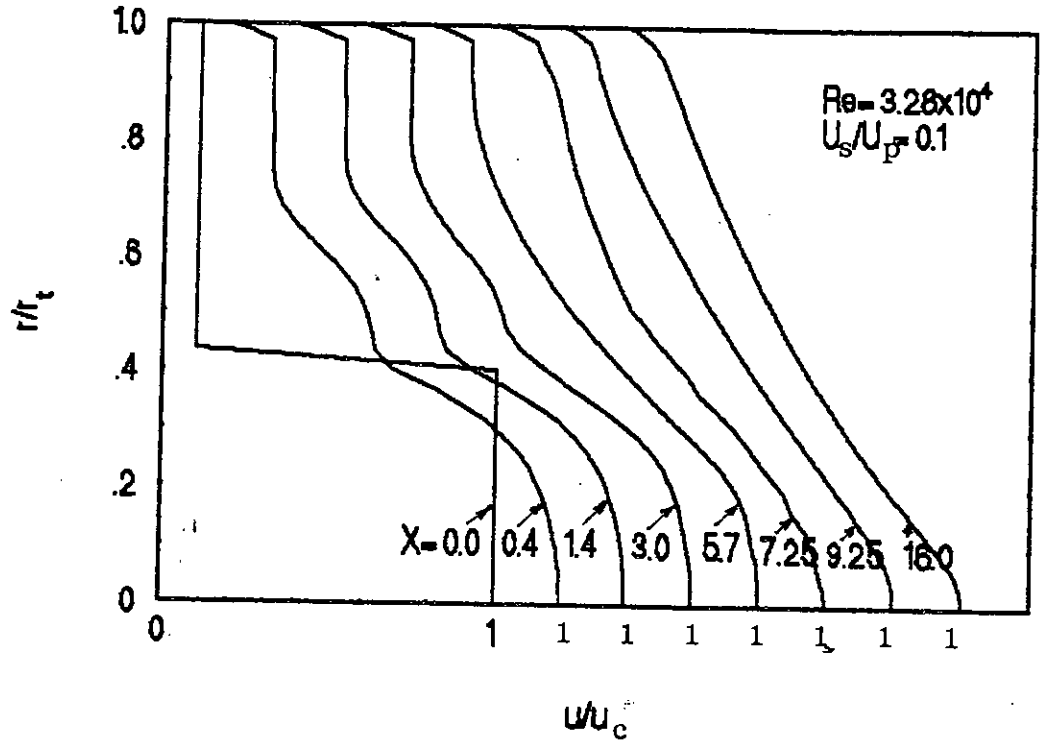

FIG:4.5b MEAN AXIAL VELOCITY(U/U_c) AT DIFFERENT AXIAL LOCATIONS FOR U_s/U_p=0.1

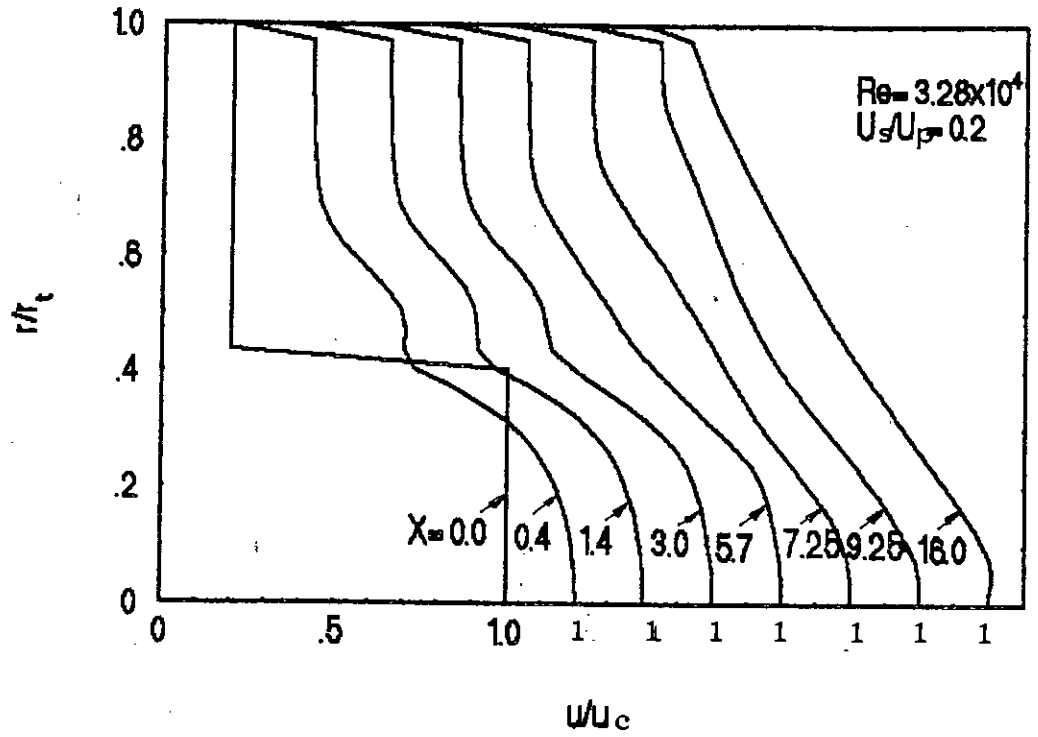

FIG: 4.5c MEAN AXIAL VELOCITY (U/U_c) AT DIFFERENT AXIAL LOCATIONS FOR U_s/U_p=0.2

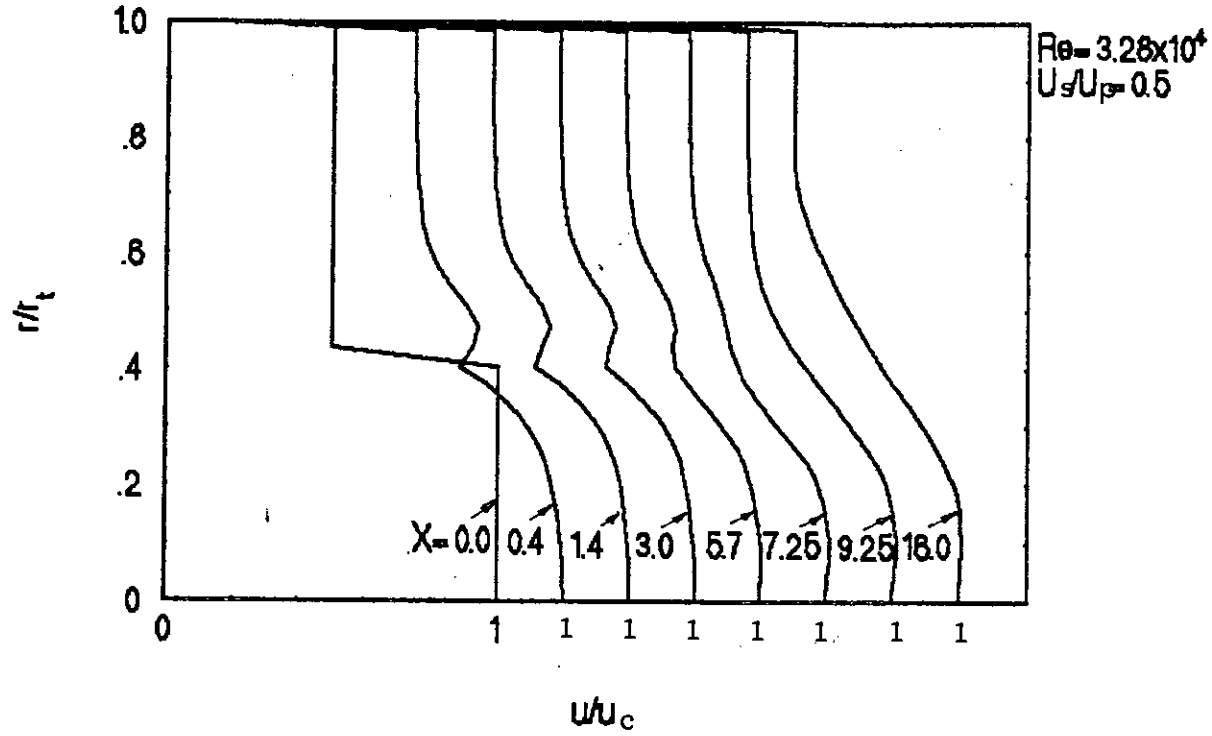

FIG: 4.5d MEAN AXIAL VELOCITY(U/U_c) AT DIFFERENT AXIAL LOCATIONS FOR U_s/U_p=0.5

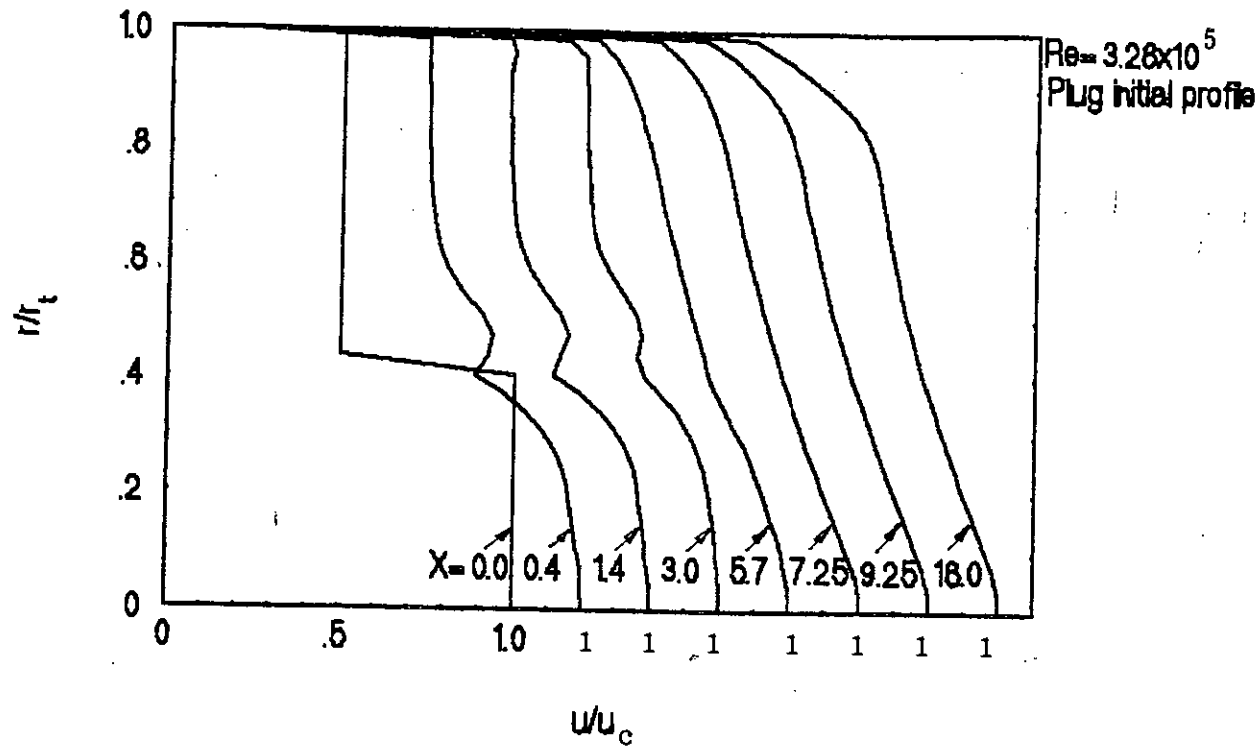

FIG: 4.6a MEAN AXIAL VELOCITY(U/U_c) AT DIFFERENT AXIAL LOCATIONS FOR PLUG INLET PROFILE

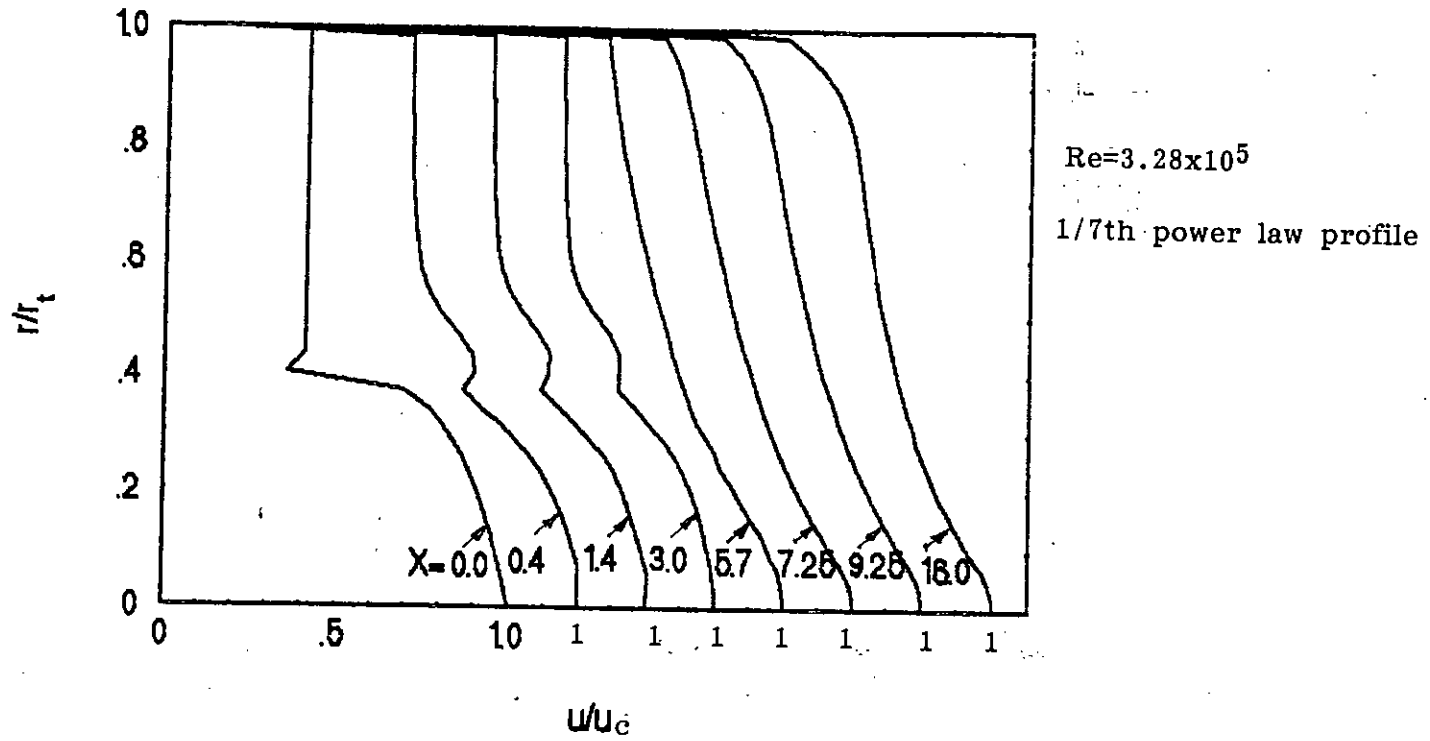

FIG: 4.6b MEAN AXIAL VELOCITY(U/U_c) AT DIFFERENT AXIAL LOCATIONS(1/7th power law profile)

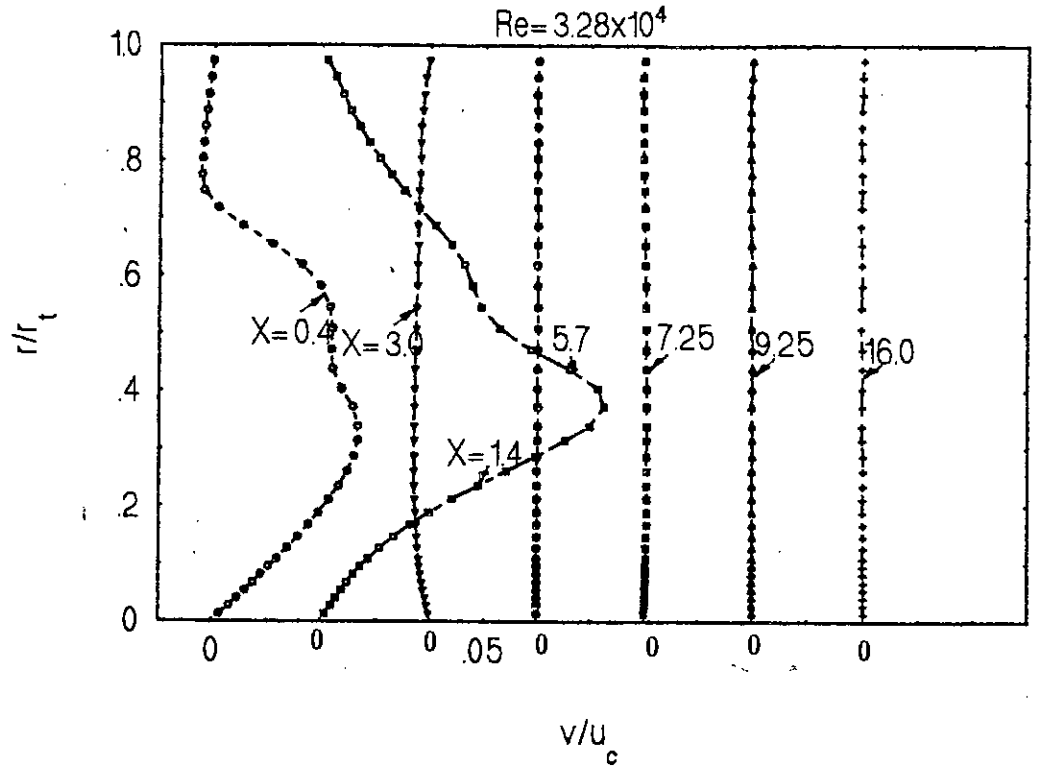

FIG: 4.7 RADIAL VELOCITY (V/U_c) AT DIFFERENT AXIAL LOCATIONS FOR INLET PROFILE = -1

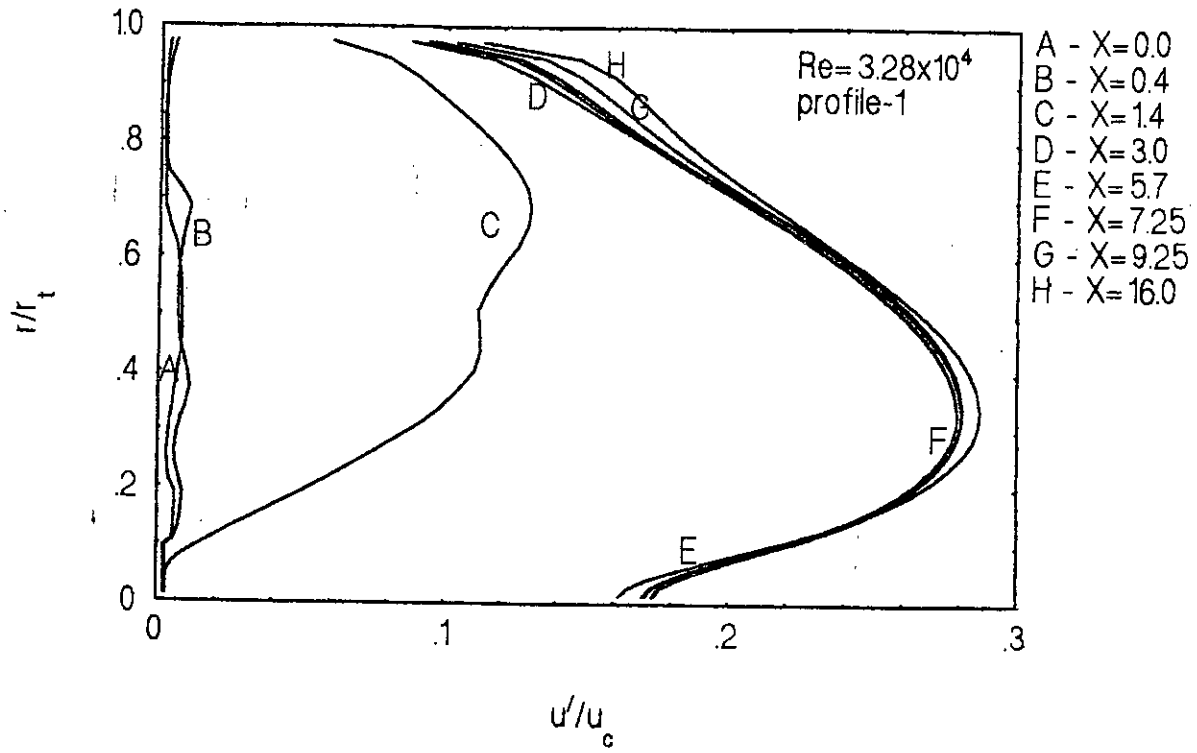

FIG: 4.8a TURBULENCE INTENSITIES AT DIFFERENT DOWNSTREAM LOCATIONS(profile-1)

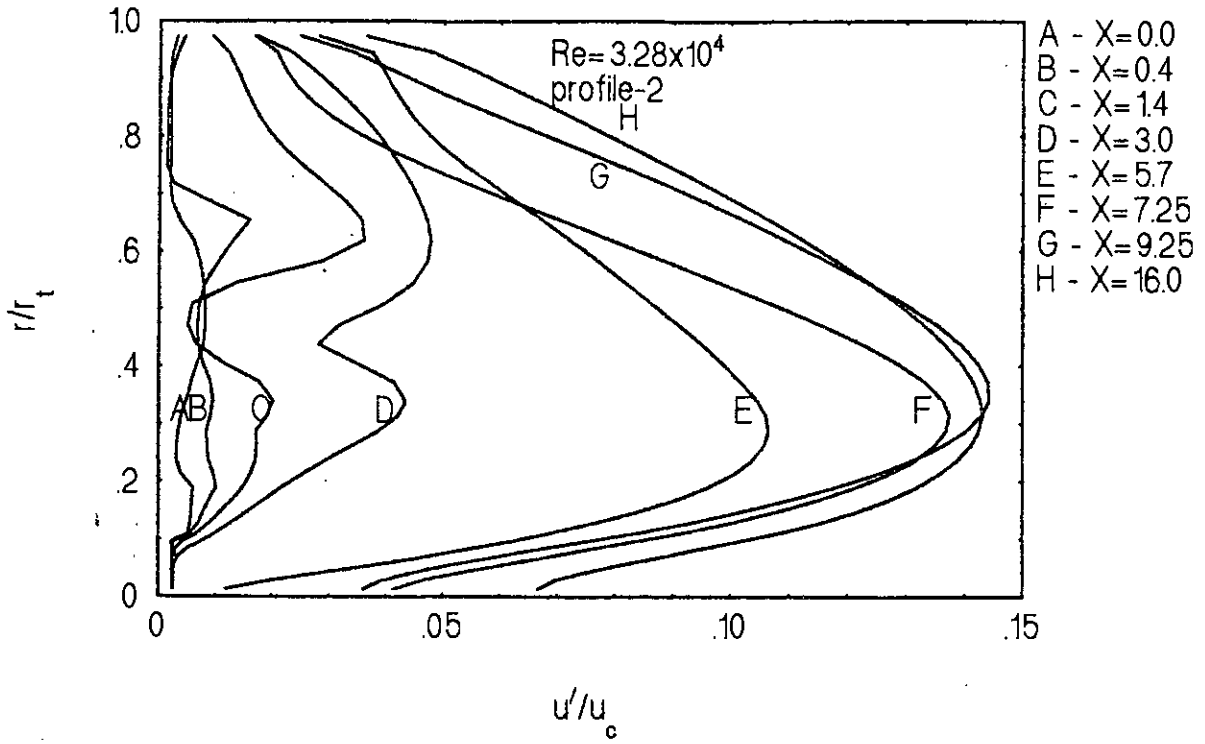

FIG: 4.8b TURBULENCE INTENSITIES AT DIFFERENT DOWNSTREAM LOCATIONS(profile-2)

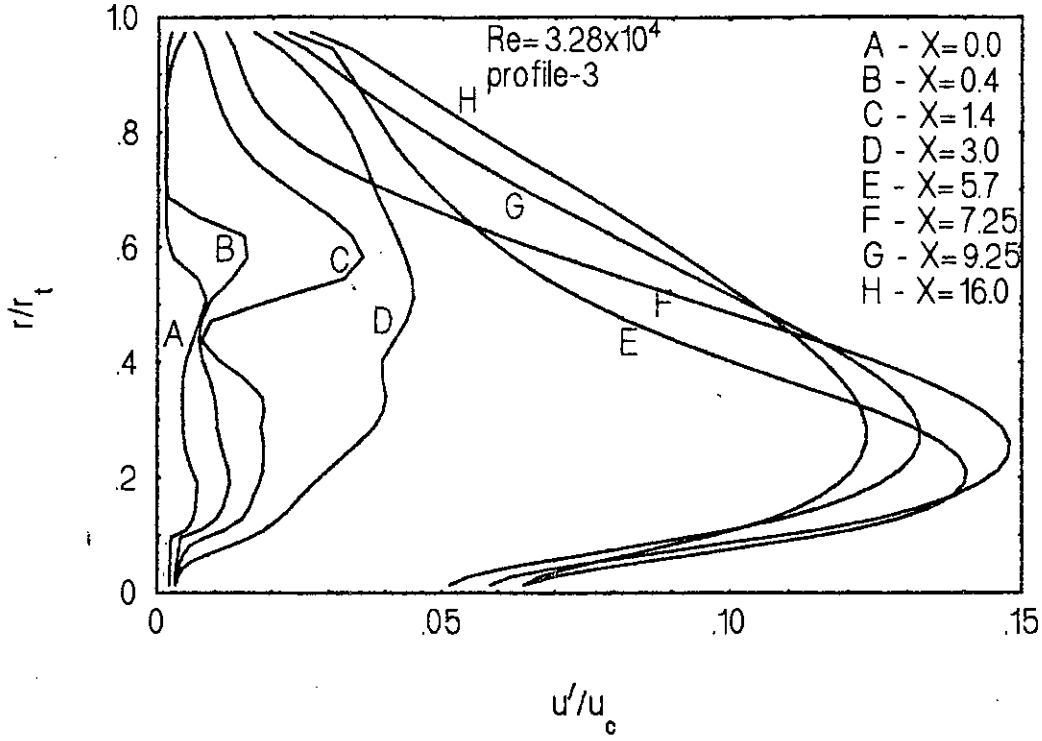

FIG: 4.8c TURBULENCE INTENSITIES AT DIFFERENT DOWNSTREM LOCATIONS(profile-3)

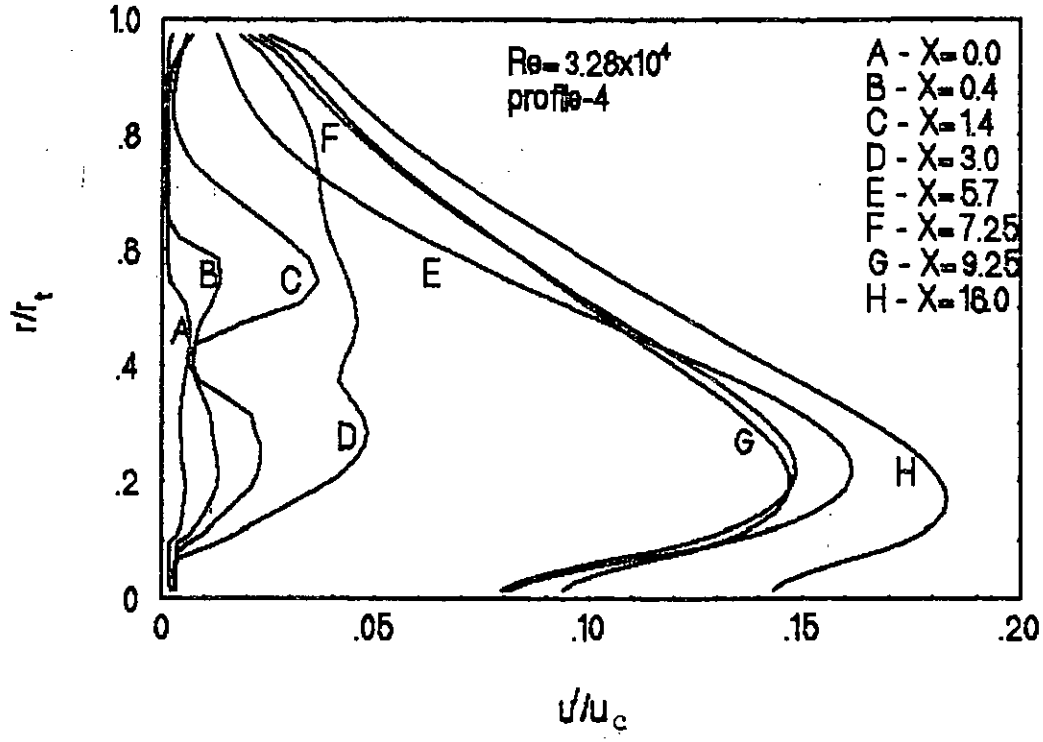

FIG: 4.8d TURBULENCE INTENSITIES AT DIFFERENT DOWNSTREAM LOCATIONS(for profile-4)

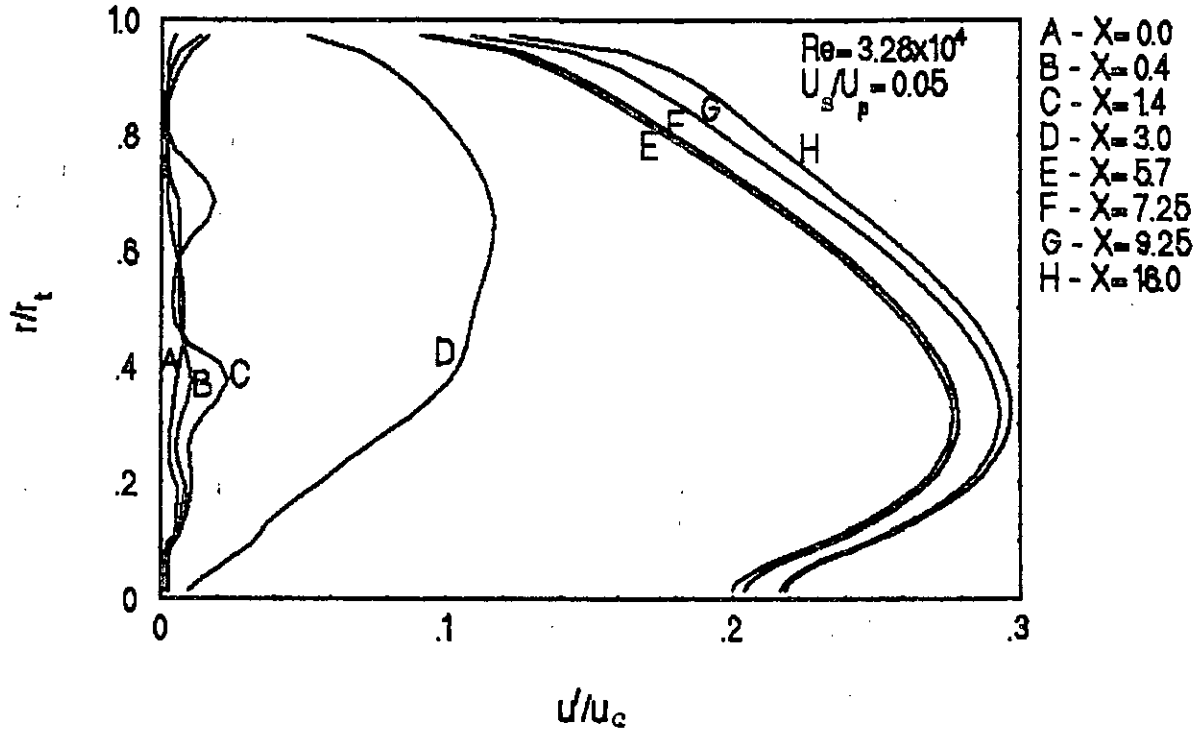

FIG: 4.9a TURBULENCE INTENSITIES AT DIFFERENT DOWNSTREAM LOCATIONS(U_s/U_p=0.05)

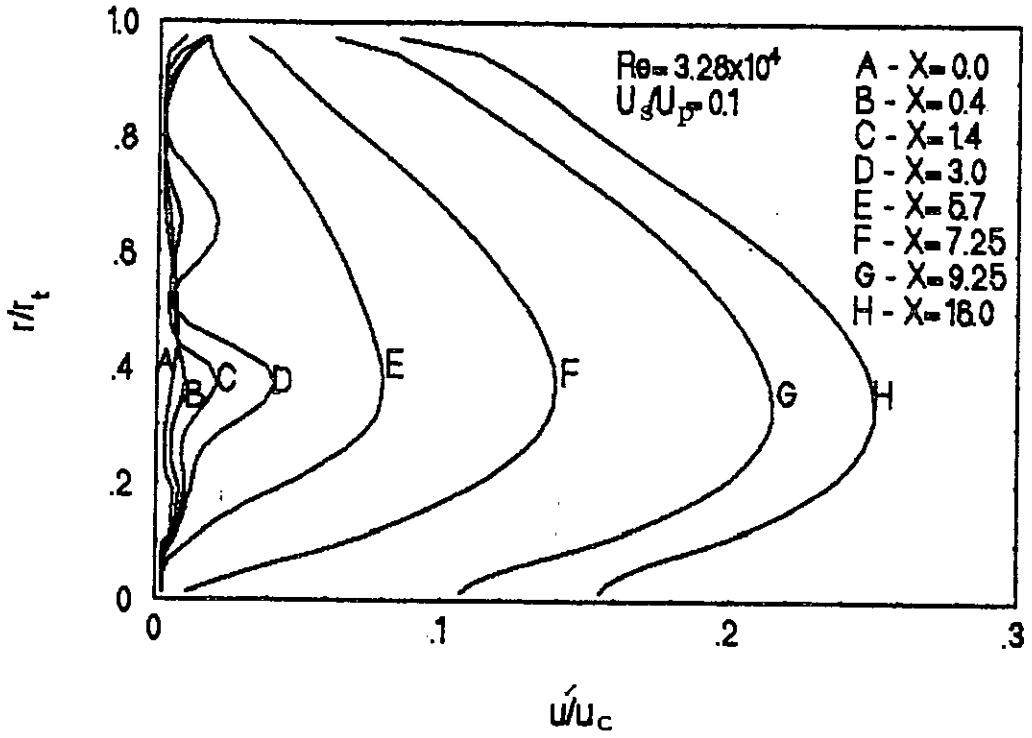

FIG:4.9b TURBULENCE INTENSITIES AT DIFFERENT DOWNSTREAM LOCATIONS (U_s/U_p=0.1)

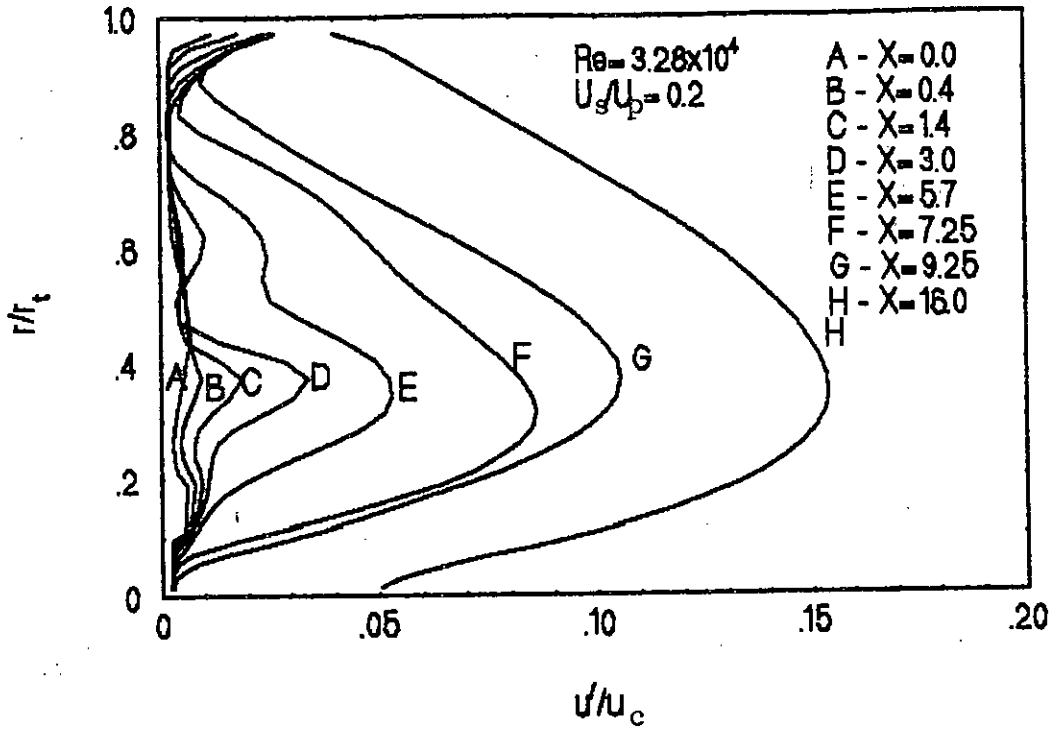

FIG: 4.9c TURBULENCE INTESITIES AT DIFFERENT DOWNSTREAM LOCATIONS(U_S/U_P=0.2)

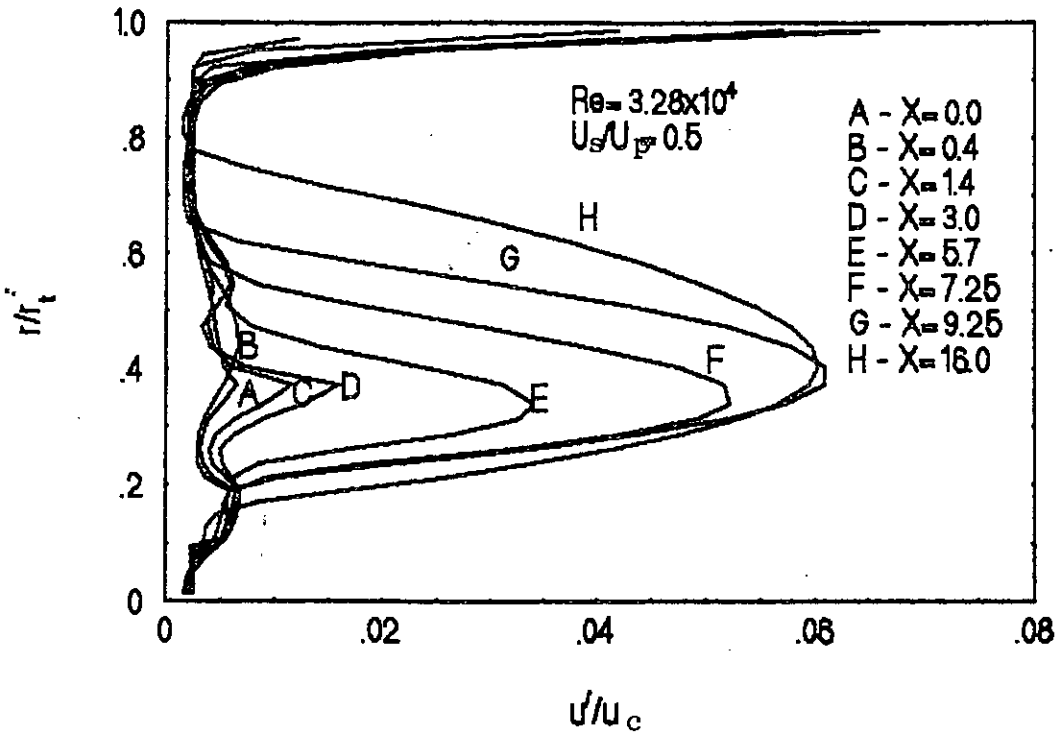

FIG: 4.9d TURBULENCE INTENSITIES AT DIFFERENT DOWNSTREAM LOCATIONS(U_S/U_p=0.5)

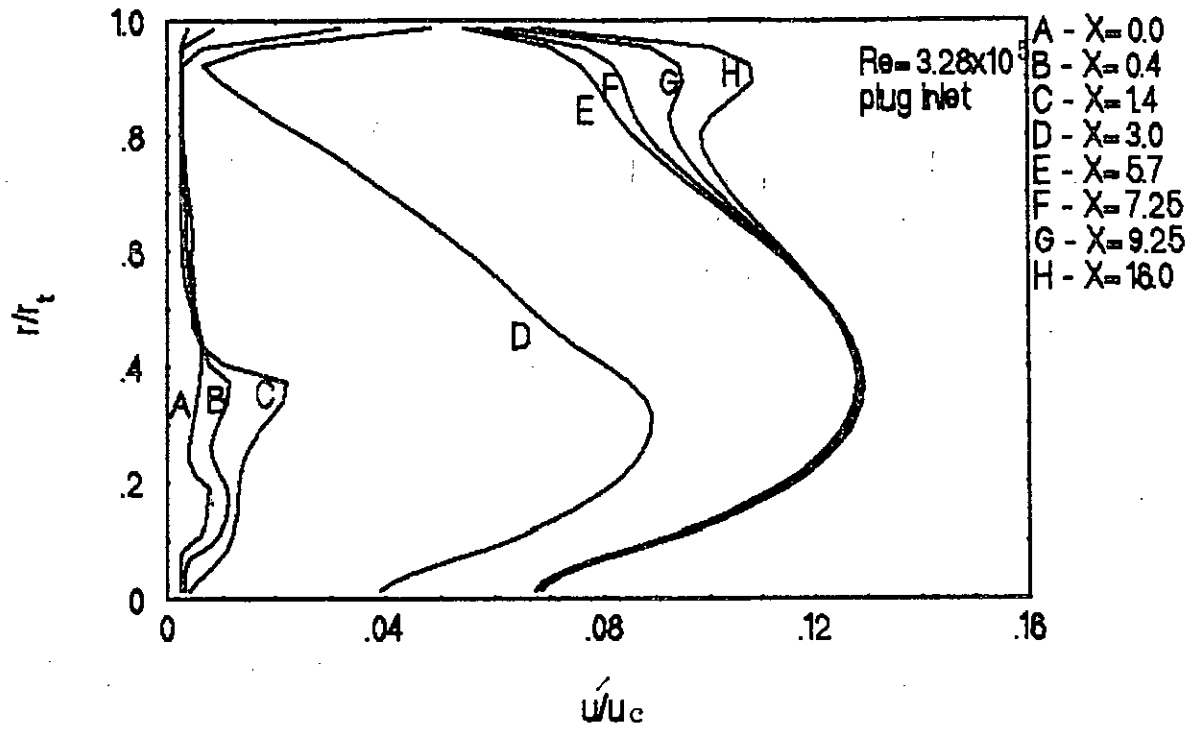

FIG: 4.10a TURBULENCE INTENSITIES AT DIFFERENT DOWNSTREAM LOCATIONS(for plug inlet profile)

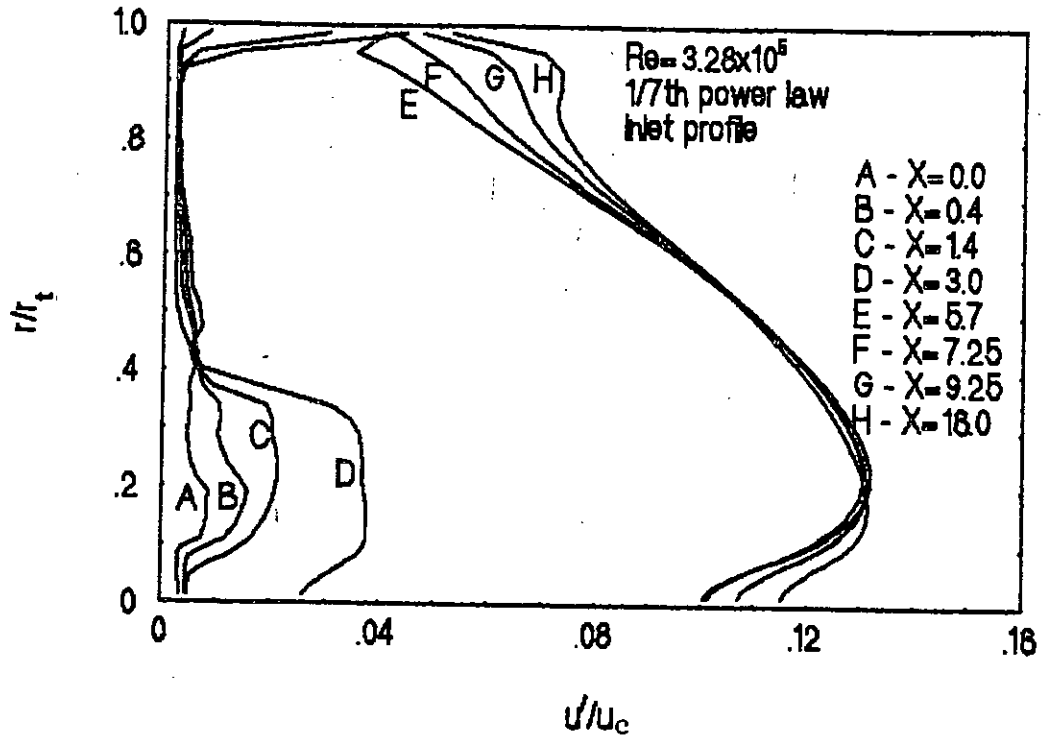

FIG: 4.10b TURBULENCE INTENSITIES AT DIFFERENT DOWNSTREAM LOCATIONS

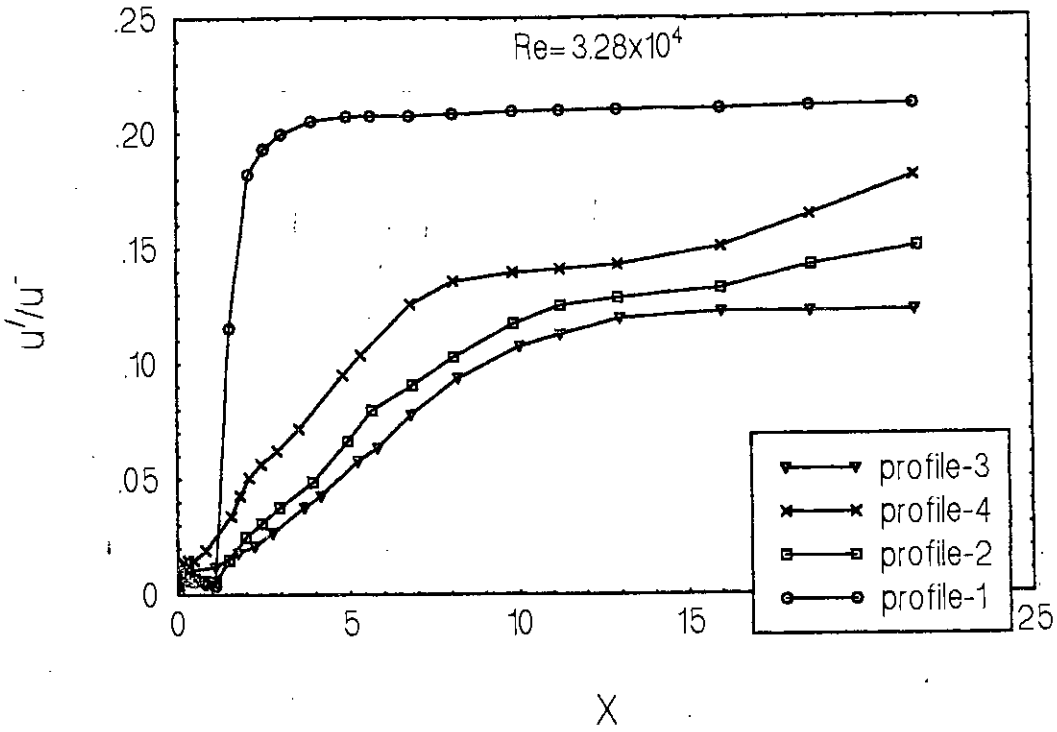

FIG:4.11 VARIATION OF TURBULENCE INTENSITIES ALONG $r_{1/2}$ FOR PROFILES 1-4.

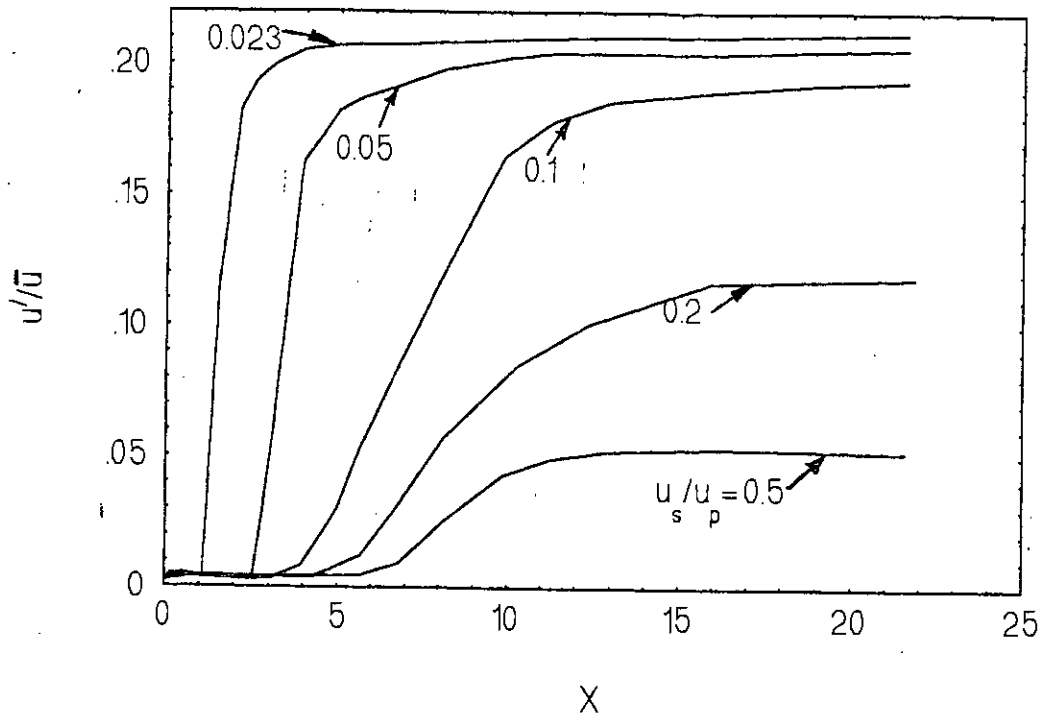

FIG: 4.12 VARIATION OF TURBULENCE INTENSITIES $r_{1/2}$ FOR DIFFERENT VELOCITIY RATIOS.

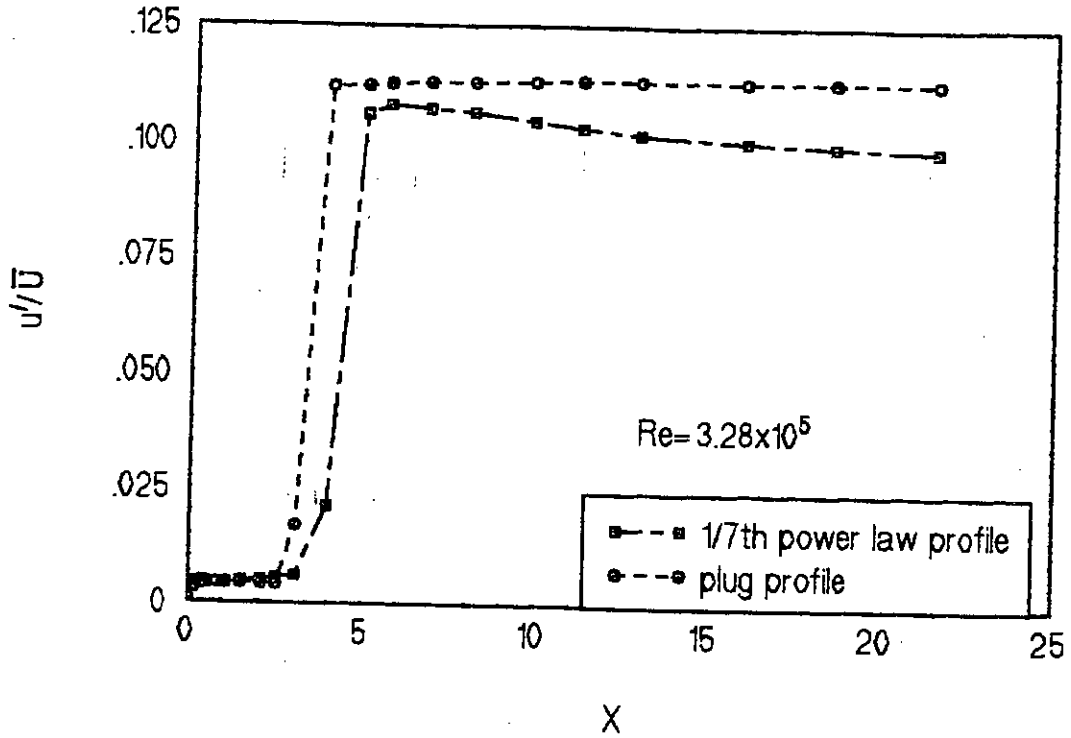

FIG: 4.13 VARIATION OF TURBULENCE INTENSITIES ALONG $r_{1/2}$ FOR PLUG & 1/7th POWER LAW PROFILE.

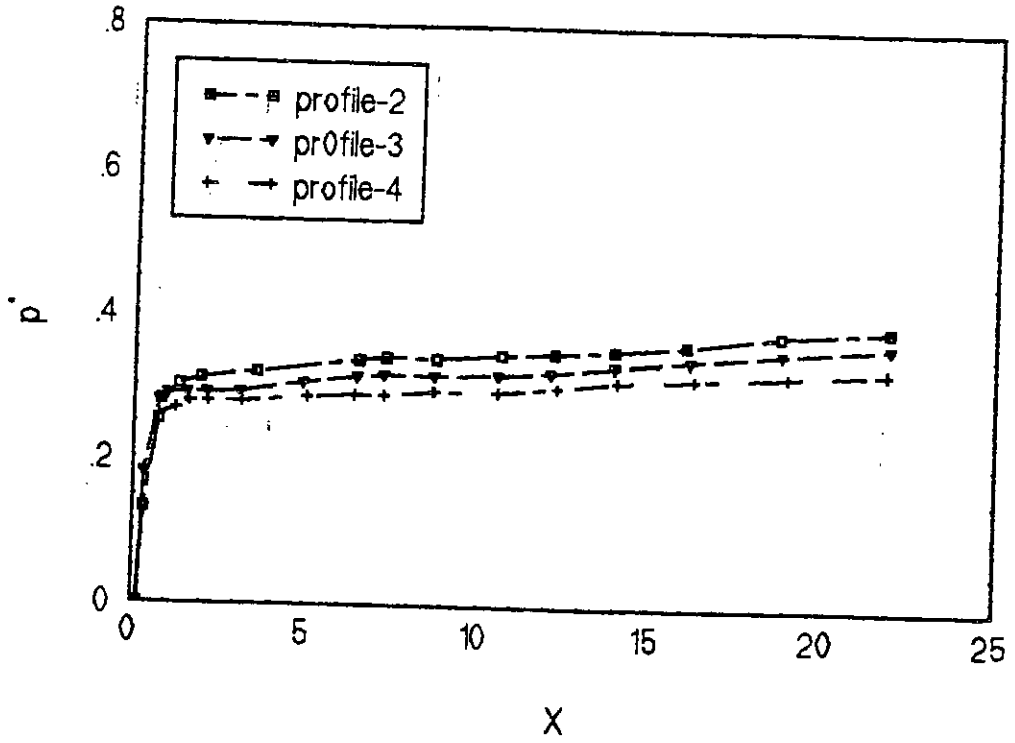

FIG:4.14 VARIATION OF STATIC PRESSURE FOR DIFFERENT INLET PROFILES(profile 2-4)

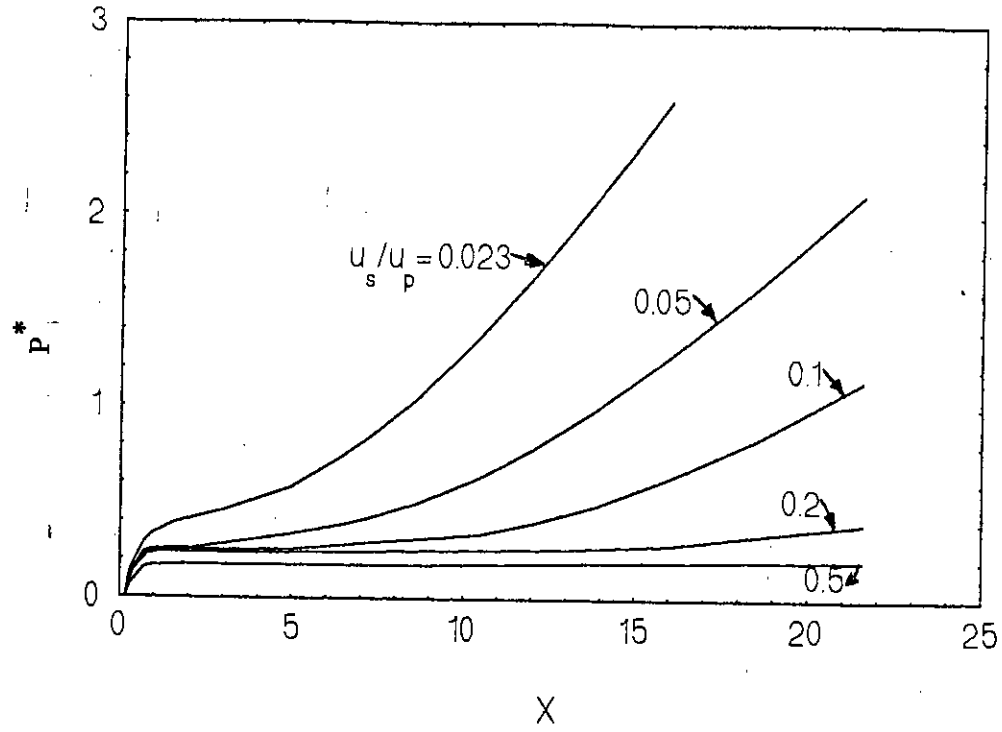

FIG: 4.15 VARIATION OF STATIC PRESSURE FOR DIFFERENT VELOCITY RATIOS

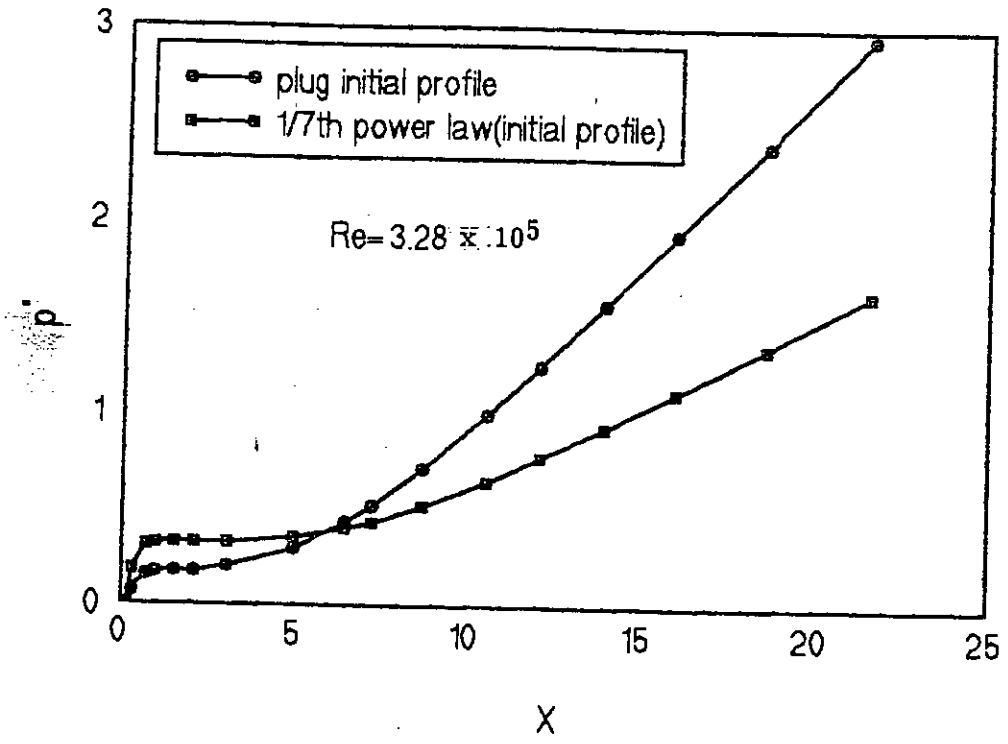

FIG. 4.16 VARIATION OF STATIC PRESSURE FOR PLUG AND 1/7 th POWER LAW PROFILE.

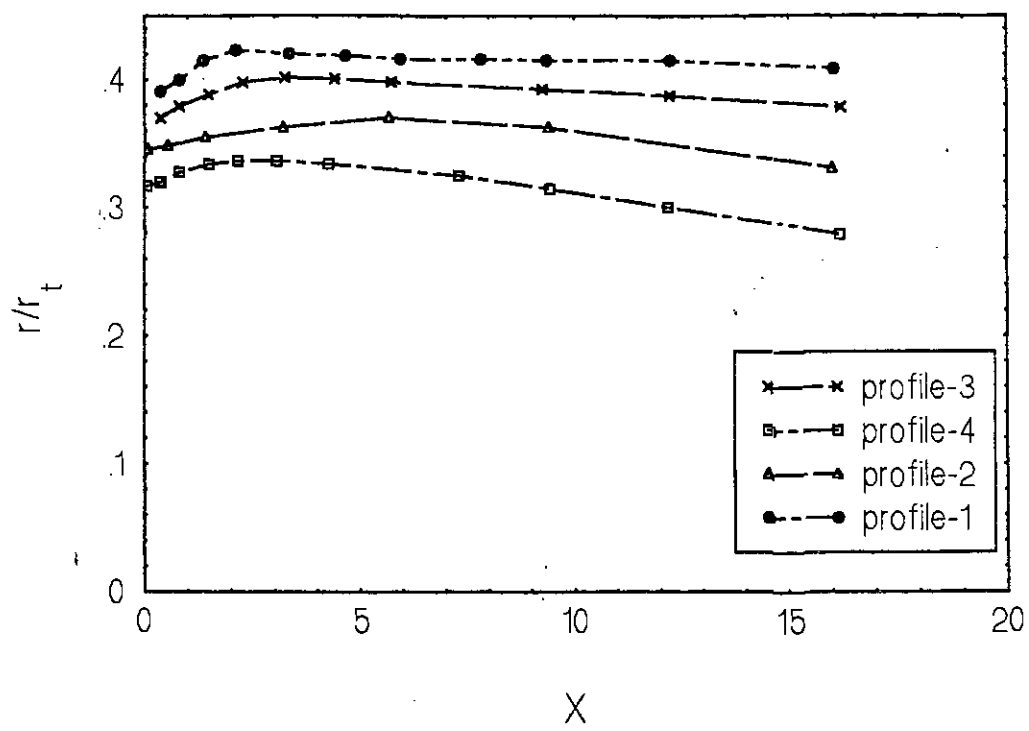

FIG: 4.17 VARIATION OF HALF RADIUS($R_{1/2}$) FOR DIFFERENT INLET PROFILE

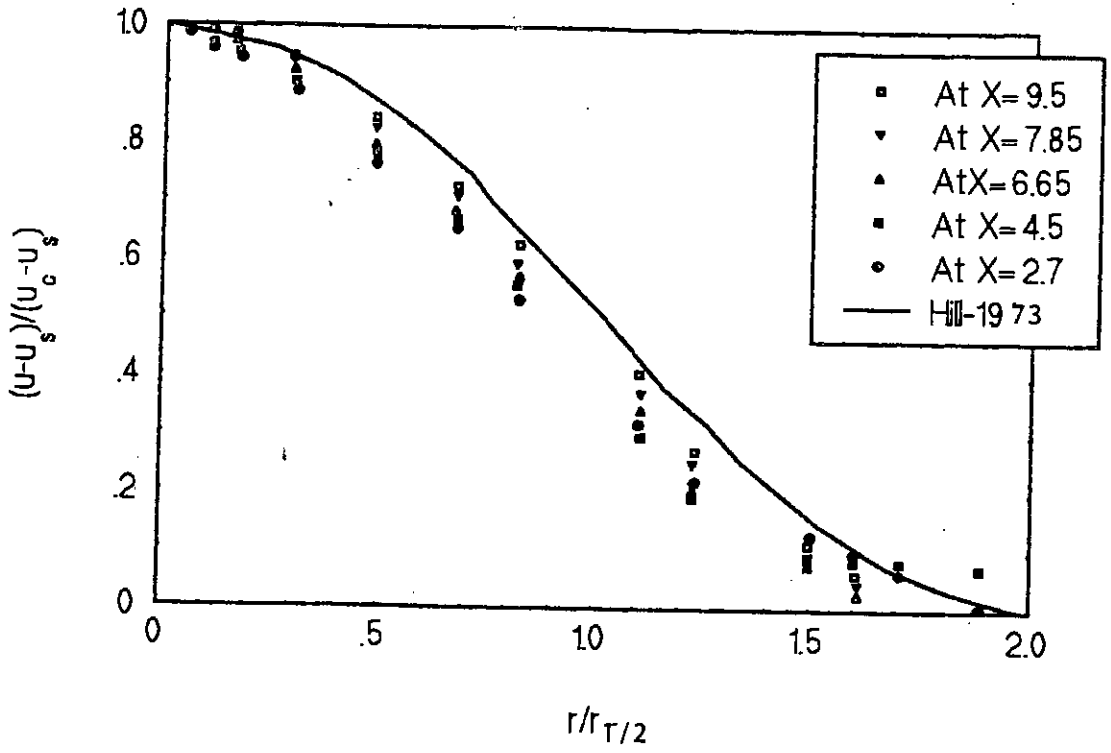

FIG:4.18 EXCESS VELOCITY PROFILE(for profile-2)

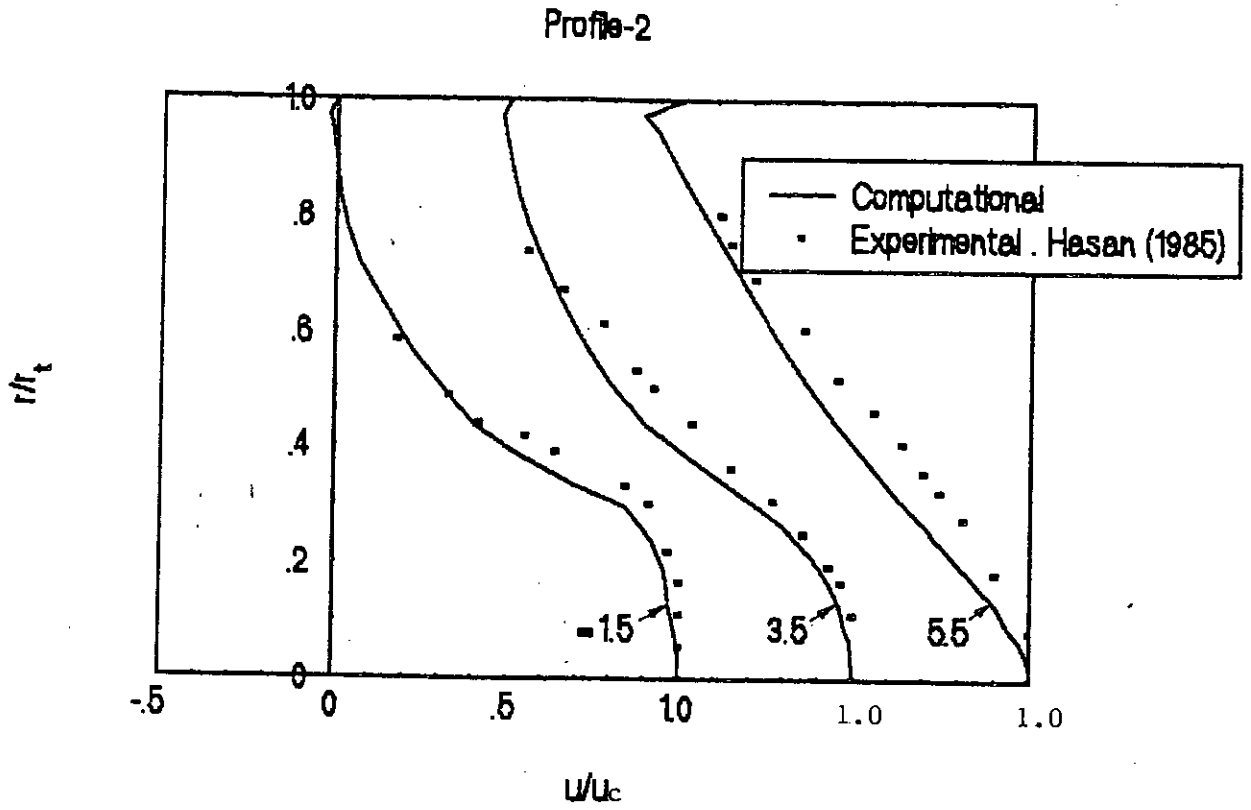

FIG: 4.19a COMPARISON OF u/u_c WITH EXPERIMENTAL RESULT FOR PROFILE-2

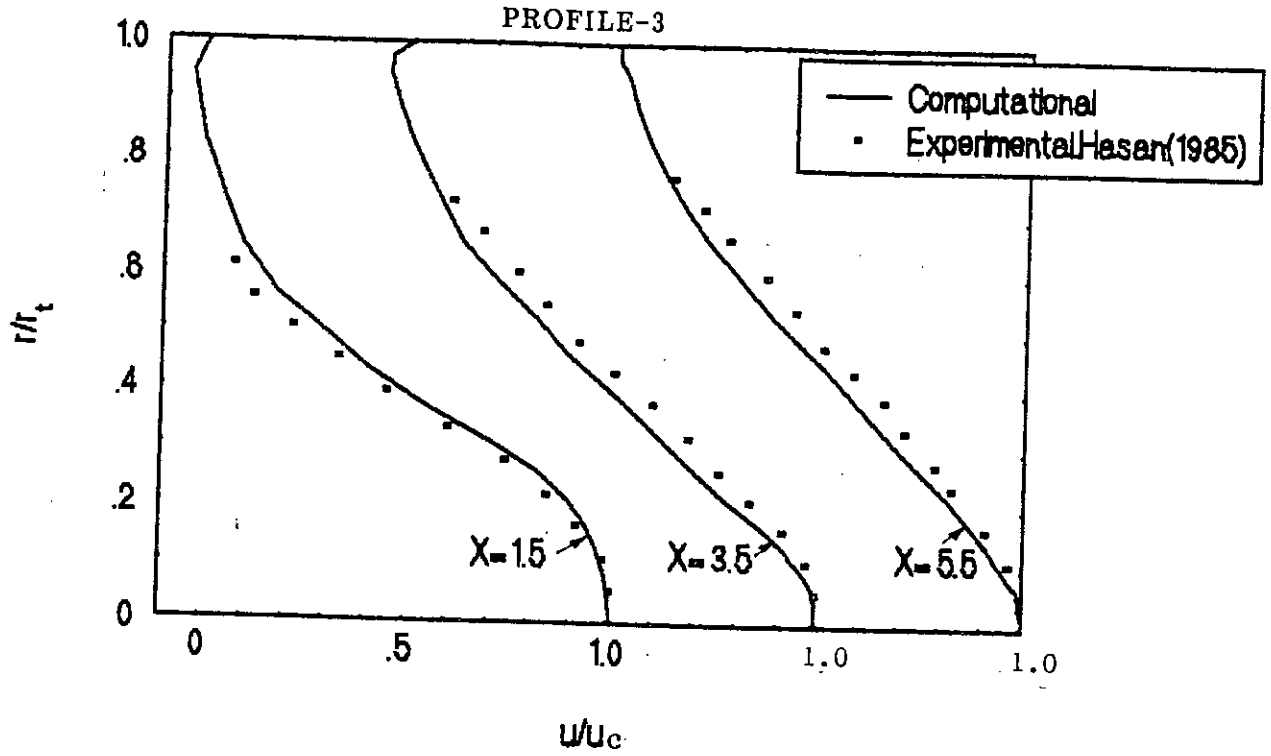

FIG: 4.19b COMPARISON OF u/u_c WITH EXPERIMENTAL RESULT FOR PROFILE-3

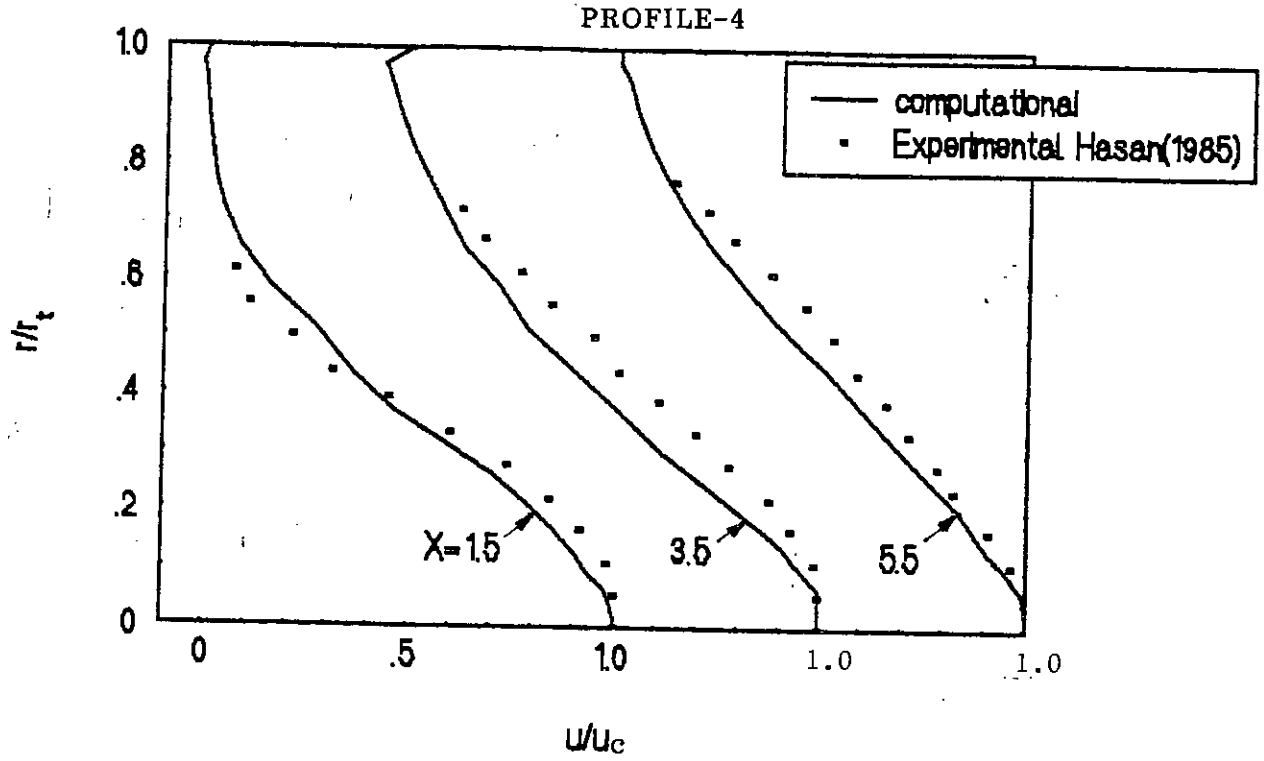

FIG: 4.19c COMPARISON OF u/u_c WITH EXPERIMENTAL RESULT FOR PROFILE-4

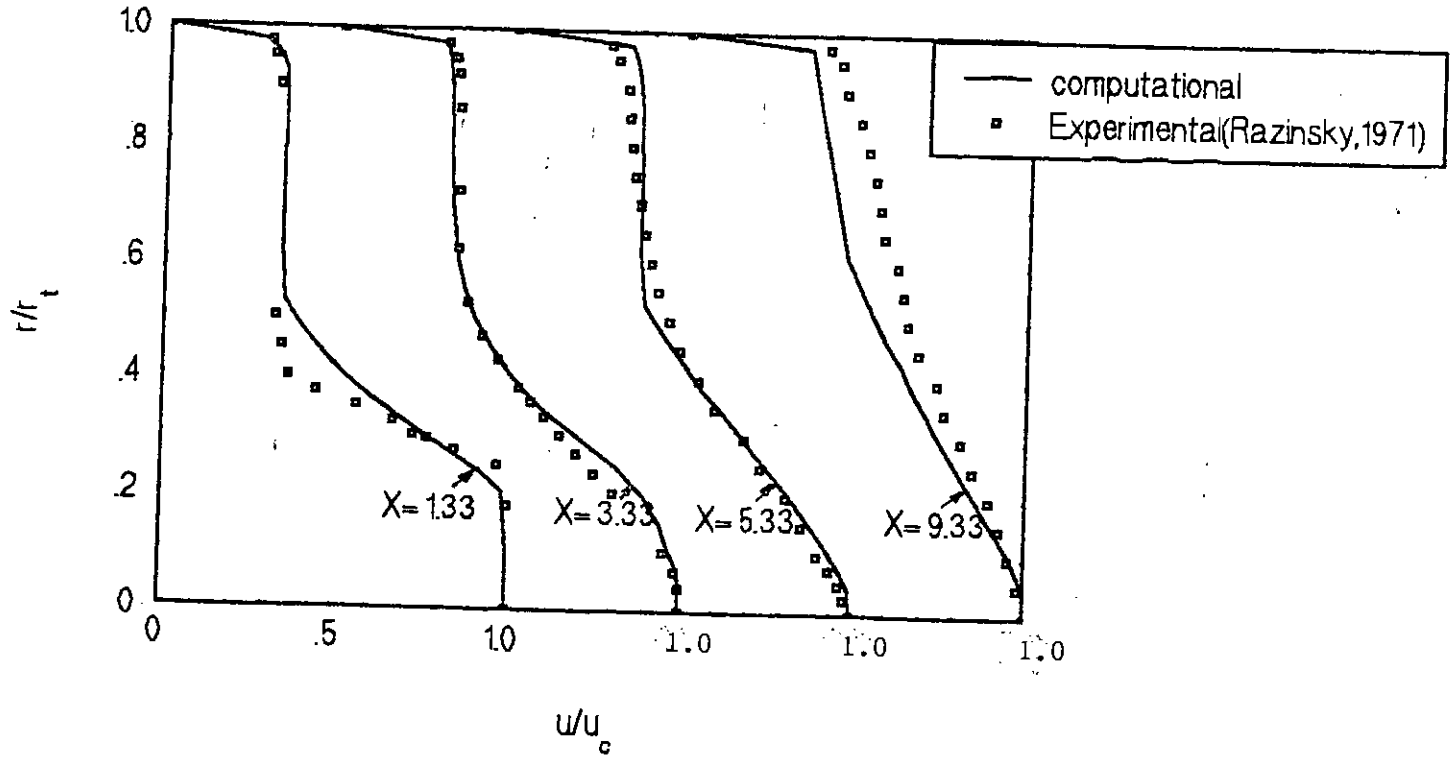

FIG:4.20 COMPARISON OF u/u_c WITH EXPERIMENTAL RESULT

APPENDIX - A

The governing Equations.

Before discussing details of the finite difference technique adopted in the available computer programme (called PACE), it is useful to record the form of the differential equations from which the difference equations are derived. These partial differential equations represent nothing more than the mathematical statements of the conservation of momentum, of energy and mass etc.

The governing equations of steady-state fluid flow in two-dimensional cylindrical polars are:-

Continuity -

$$\frac{1}{r}\frac{\partial}{\partial r}(\rho r V) + \frac{\partial}{\partial x}(\rho u) = 0 \qquad [A1]$$

u-momentum

$$\frac{1}{r}\frac{\partial}{\partial r}(\rho u v r) + \frac{\partial}{\partial x}(\rho u^2)$$

$$= -\frac{\partial}{\partial x}(P + \frac{2}{3}\mu\theta) + \frac{1}{r}\frac{\partial}{\partial r}\{\mu r(\frac{\partial v}{\partial x} + \frac{\partial u}{\partial r})\}$$

$$+ \frac{1}{r}\frac{\partial}{\partial \phi}(\frac{\mu}{r}\frac{\partial u}{\partial \phi}) + 2\frac{\partial}{\partial x}(\mu\frac{\partial u}{\partial x}) \qquad [A2]$$

Where, θ is the dilation, and represent as follows:

$$\theta = \frac{1}{r}\frac{\partial}{\partial r}(rv) + \frac{\partial u}{\partial x}$$

V-Momentum

$$\frac{1}{r}\frac{\partial}{\partial r}(\rho v^2 r) + \frac{\partial}{\partial x}(\rho v u)$$

$$= -\frac{\partial}{\partial r}(P + \frac{2}{3}\mu\theta) + \frac{2}{r}\frac{\partial}{\partial r}(\mu r\frac{\partial v}{\partial r})$$

$$+ \frac{1}{r}\frac{\partial}{\partial \phi}(\frac{\mu}{r}\frac{\partial v}{\partial \phi}) + \frac{\partial}{\partial x}\{\mu(\frac{\partial v}{\partial x} + \frac{\partial u}{\partial r})\} - \frac{2}{r^2}\mu v \qquad [A3]$$

Now as the flow geometry is axisymmetric cylindrical coordinate is used in this study. For cylindrical coordinate ϕ term is dropped from the equations. Hence the governing equations are thus written in cylindrical co-ordinate which are as follows:

Continuity $$\frac{1}{r}\frac{\partial}{\partial r}(\rho r v) + \frac{\partial}{\partial x}(\rho u) = 0 \qquad [A4]$$

U-momentum $$\frac{1}{r}\frac{\partial}{\partial r}(\rho r v u) + \frac{\partial}{\partial x}(\rho u^2)$$

$$= -\frac{\partial}{\partial x}(P + \frac{2}{3}\mu\theta) + \frac{1}{r}\frac{\partial}{\partial r}\{\mu r(\frac{\partial v}{\partial x} + \frac{\partial u}{\partial v})\} + 2\frac{\partial}{\partial x}(\mu\frac{\partial u}{\partial x}) \qquad [A5]$$

V-Momentum $\frac{1}{r}\frac{\partial}{\partial r}(\rho r v^2) + \frac{\partial}{\partial x}(\rho u v)$

$$= -\frac{\partial}{\partial r}(P + \frac{2}{3}\mu\theta) + \frac{2}{r}\frac{\partial}{\partial r}(\mu r \frac{\partial v}{\partial r} + \frac{\partial}{\partial x}\{\mu(\frac{\partial v}{\partial x} + \frac{\partial u}{\partial r})\} - \frac{2}{r^2}\mu v \qquad [A6]$$

Now by putting the value of dilation θ and simplifying equations [A4], [A5] and [A6] the equations can be represents by one single equation with a general variable Ψ as equation 3.1 presented in chapter 3.

APPENDIX - B

Detailed About Computer Programming

Calculation of the flow field:

The differential equations of the flow fields as described in Chapter-3 are descretised over the cell volume. The control volume for discretization shown in Fig. 3.2. The resulting discretization equation for U (Eq. A5) can be written as

$$a_e U_e = \sum a_{nb} U_{nb} + S_e \qquad [B.1]$$

Where the a_{nb} are coefficients multiplying the values of U at the neighbour nodes surrounding the central node P, a_e is the coefficient of V_e and S_e containes all other terms which are not expressed through the nodal values of the dependent variable (e.g. the source term, pressure gradients etc.). The coefficients a_{nb} contain combined convection-diffusion influence at the control-volume faces. In equation B.1 S_e can be represented as follows:

$$S_e = b + (P_P - P_E) A_e \qquad [B.2]$$

Here the term $(P_p - P_E)$ is the pressure gradient between nodes P and E. A_e is area of the control volume and hence $(P_P - p_E) A_e$ represents the pressure force acting on the control volume face.

The momentum equations can be solved only when the pressure field is known or somehow estimated. Unless the correct pressure field is employed, the resulting velocity field will not satisfy the continuity equation. Hence in order to start the iterative procedure, a pressure field is first estimated for the flow domain. The resulting imperfect velocity field based on guessed pressure field p^* will be denoted u^*. This "Starred" velocity field will result from the solution of the following discretization equations:

$$a_e u_e^* = \sum (a_{nb} U_{nb}^*) + b + (P_P^* - P_E^*) A_e \qquad [B.3]$$

The pressure and Velocity Corrections:

The main objective is to improve the guess pressures p^* such that the resulting "Starred" velocity field will progressively get closer to satisfying the continuity equation.

Let the corrected pressure P is obtained from the following relation:

$$P = P^* + P' \qquad [B.4]$$

Where P' is the pressure correction. the corresponding velocity correction can be introduced as;

$$U = U^* U' \qquad [B.5]$$

Subtracting eq. [B.3] from [B.1],

$$a_e U'_e = \sum a_{nb} U'_{nb} + (P'_P - P'_E) A_e \qquad [B.6]$$

Dropping the term $\sum a_{nb} U'_{nb}$ from equation [B.6] for computational convenience (Patankar[24]), Eq. [B.6] becomes

$$a_e U'_e = (P'_P - P'_E) A_e$$

or,

$$U'_e = d_e (P'_P - P'_E) \qquad [B.7]$$

Where $d_e = A_e/a_e$

Equation [B.7] will be the velocity-correction formula, which can also be written as-

$$U_e = U^*_e + d_e (P'_P - P'_E) \qquad [B.8]$$

Similarly, for V-velocity,

$$V_n = V^*_e + d_n (P'_P - P'_N) \qquad [B.9]$$

The pressure correction equation can be obtained from the continuity equation.

The continuity equation is

$$\frac{\partial}{\partial x}(\rho u) + \frac{\partial}{\partial y}(\rho V) = 0 \qquad [B.10]$$

Substituting the velocity components from equation [B.8] and [B.9], the discretization equation for P.

$$a_P P'_P = a_E P'_E + a_w P'_w + a_N P'_N + a_s P'_s + b \qquad [B.11]$$

Solution Procedure:

For the calculation of the flow field, the algorithum used in the entire solution is SIMPLE (Semi-Implicit Method for Pressure-Linked Equations). The important operations in the order of their execution, are:

1. Guess the pressure field P^*.
2. Solve the momentum equations, to obtain u^*, v^*.
3. Solve the P' equation.
4. Calculate P from Eq. [B.4] by adding P to P^*.
5. Calculate U, V from their starred values using the velocity-correction formulas [B.8] and [B.9].
6. Solve the discretization equation for other variables (such as turbulence quantities) if they influence the flow field.
7. Treat the corrected pressure P as a new guessed pressure p^*, return to step 2, and repeat the whole procedure until a converged solution is obtained.

General Structure of the Computer Programme:

The computer programme PACE solves the partial differential conservation equations for two-dimensional flows. The programme is divided into some subroutines. These fall into two groups; namely (1) those which are related to the basic finite difference method and which require no change and (2) those which are problem dependent and concerned with input, specification of boundary conditions and output from the programme etc.

The subroutines MAIN, BLOCK DATA, PROBSP and OUTPUT are problem dependent and other subroutines such as COEFF, SOLVER,SOURCE, TRANSP, TEST etc., are problem independent. The purpose of the various subroutines are briefly described below. The layout of the programme is schematically shown in Fig. B1.

MAIN

Main is primarily a co-ordinating subroutine which is responsible for transferring control to and from other routines. It also terminates the calculation at the appropriate point.

BLOCK DATA

This routine is used to input various universal constants, output titles and

programme controlling parameters etc.

PROBSP

The boundary conditions are specified in this subroutine.

OUTPUT

Output is the subroutine which prints out the values of all the computed variables.

COEFF

The purpose of COEFF is to setup the finite difference coefficients such as a_e in Eq. B1 for each variable. It is subdivided into three sections. First two of these, are called once only and serve to setup various geometric coefficients. In the third section, the algebraic coefficients needed for the numerical integration of transport equations are calculated.

SOURCE

In this subroutine the source (i.e. net formation rate) per unit volume is calculated for each dependent variable. The routine is arranged with sections for each of the variables being considered.

TRANSP

This routine servs the purpose of calculating the diffusion coefficients appropriate to the conservation equation being solved.

TEST

The purpose of TEST is to print out various diagnostic output if required. The values of the finite difference coefficients, the diffusion coefficients and the source terms are printed out at various stages during a calculation cycle.

SOLVER

Solver performs the task of solving the set of algebraic equations, the coefficients of which are set in COEFF and SOURCE.

COMPUTER PROGRAMME FLOW CHART

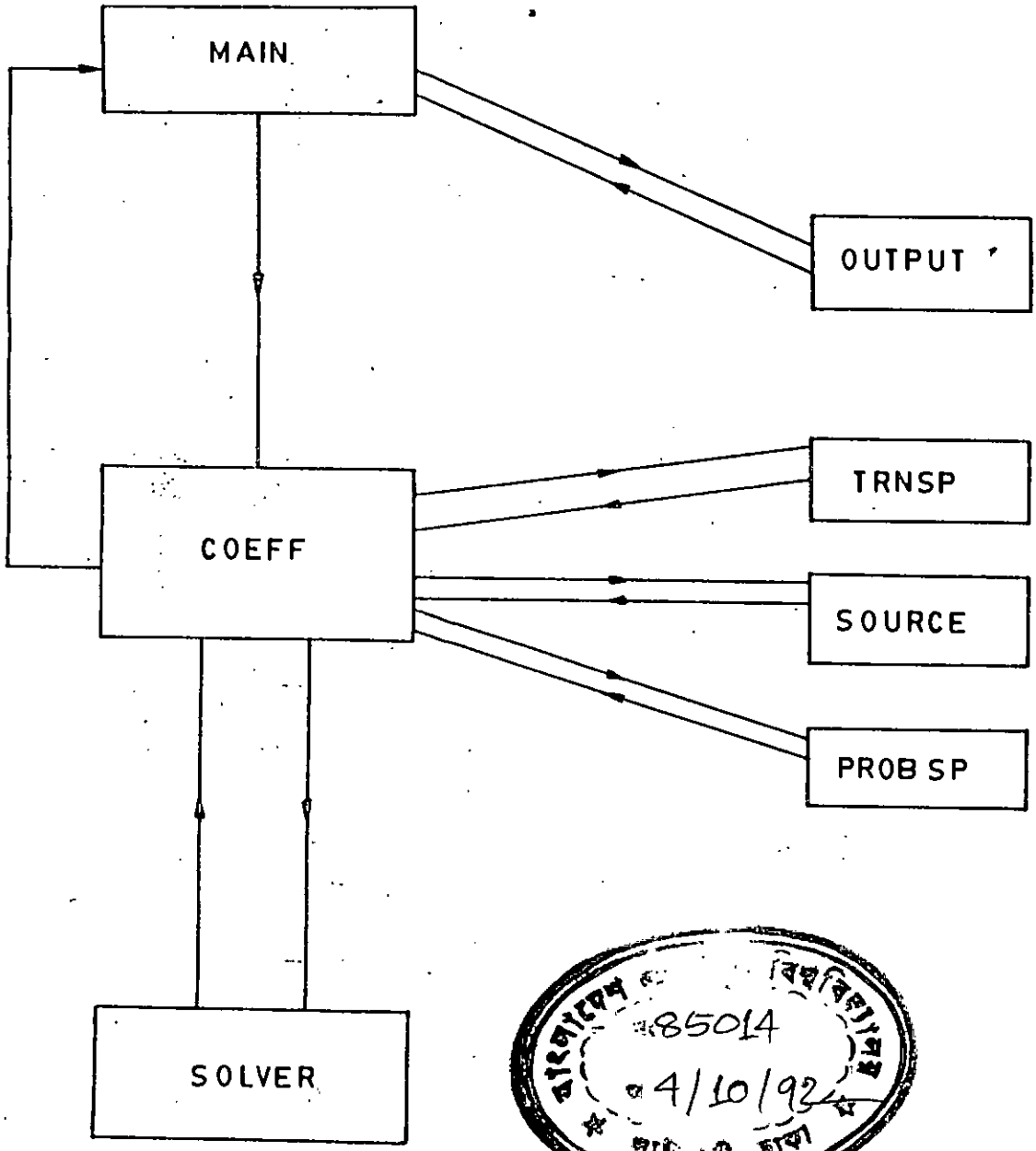

FIG. B1